Plant Cell Reports

Kinetin Induces Microtubular Breakdown, Cell Cycle Arrest and Programmed Cell Death in Tobacco BY-2 Cells

--Manuscript Draft--

Manuscript Number:		
Full Title:	Kinetin Induces Microtubular Breakdown, Cell Cycle Arrest and Programmed Cell Death in Tobacco BY-2 Cells	
Article Type:	Original Article	
Funding Information:	university of łódź (1409)	Prof. Dr. Andrzej Kaźmierczak
Abstract:	Plant cells can undergo regulated cell death in response to exogenous factors (often in a stress context), but also as regular element of development (often regulated by phytohormones). The cellular aspects of these death responses differ, which implies that the early signalling must be different. We use cytokinin-induced programmed cell death as paradigm to get insight into the role of the cytoskeleton for the regulation of developmentally induced cell death, using tobacco BY-2 cells as experimental model. We show that this PCD in response to kinetin correlates with an arrest of the cell cycle, a deregulation of DNA replication, a loss of plasma membrane integrity, a subsequent permeabilisation of the nuclear envelope, an increase of cytosolic calcium, a suppression of callose deposition, and a complete loss of microtubule integrity, while actin microfilaments persist. We discuss these findings in the context of a working model, where kinetin, mediated by calcium, causes the breakdown of the microtubule network, which, either by release of executing proteins, or by mitotic catastrophe, will result in PCD. (171 words).	
Corresponding Author:	Peter Nick Botanical Institute, Karlsruhe Institute of Technology GERMANY	
Corresponding Author Secondary Information:		
Corresponding Author's Institution:	Botanical Institute, Karlsruhe Institute of Technology	
Corresponding Author's Secondary Institution:		
First Author:	Andrzej Kaźmierczak	
First Author Secondary Information:		
Order of Authors:	Andrzej Kaźmierczak	
	Eva Siatkowska	
	Ruoxi Li	
	Sophie Bothe	
	Peter Nick	
Order of Authors Secondary Information:		
Author Comments:	none	
Suggested Reviewers:		

Kinetin Induces Microtubular Breakdown, Cell Cycle Arrest and Programmed Cell Death in Tobacco BY-2 Cells

Andrzej Kaźmierczak[1,2], Ewa Siatkowska[1], Ruoxi Li[2], Sophie Bothe[2], Peter Nick[2,*]

[1] University of Łódź, Faculty of Biology and Environmental Protection, Institute of Experimental Biology, Department of Cytophysiology, Pomorska 141/143, 90-236 Łódź, Poland

[2] Botanical Institute, Karlsruhe Institute of Technology, Fritz-Haber-Weg 4, D-76131 Karlsruhe, Germany.

*** Correspondence:** Peter Nick, peter.nick@kit.edu. ORCID: 0000-0002-0763-4175

Funding The work was funded by grant 1409 from the University of Łódź to AK.

Conflicts of interest/Competing interests: none.

Availability of data and material: The datasets presented in this study are stored on the server of the Steinbuch Centre for Computing and are made available on reasonable request.

Authors' contributions: AK conducted most of the experiments, analysed the data and wrote part of the manuscript, ES, RL, and SB participated in the experiments, PN wrote part of the manuscript, compiled the figures, and edited.

Key Message

Kinetin can induce programmed cell death in tobacco BY-2 cells linked with a breakdown of the microtubular cytoskeleton, cell-cycle arrest and perturbed DNA replication (24 words).

Keywords: Callose, Cell cycle arrest, kinetin, microtubules, Programmed Cell Death, Tobacco BY-2

Abstract. Plant cells can undergo regulated cell death in response to exogenous factors (often in a stress context), but also as regular element of development (often regulated by phytohormones). The cellular aspects of these death responses differ, which implies that the early signalling must be different. We use cytokinin-induced programmed cell death as paradigm to get insight into the role of the cytoskeleton for the regulation of developmentally induced cell death, using tobacco BY-2 cells as experimental model. We show that this PCD in response to kinetin correlates with an arrest of the cell cycle, a deregulation of DNA replication, a loss of plasma membrane integrity, a subsequent permeabilisation of the nuclear envelope, an increase of cytosolic calcium, a suppression of callose deposition, and a complete loss of microtubule integrity, while actin microfilaments persist. We discuss these findings in the context of a working model, where kinetin, mediated by calcium, causes the breakdown of the microtubule network, which, either by release of executing proteins, or by mitotic catastrophe, will result in PCD. (171 words).

1 Introduction

Although self-perpetuation represents a central (possibly the central) feature for living beings, death can occur not just as accidental byproduct of damage or perturbation but can be initiated actively. This regulated form of cell death is, in fact, one of the most important processes controlling differentiation of plants (reviewed in Lam 2004; Locato and de Gara 2018), animals (Galluzzi et al. 2018), as well as of prokaryotic organisms (Tanouchi et al. 2013). Although terminating life of the individual cell, this phenomenon can be essential for the survival of the entire organism (or the cell population in case of unicellular life forms). The functions of regulated cell death are manifold – the removal of damaged cells, as to improve resource allocation to their intact neighbours, or the active self-elimination to provide material or signals for the development of other cells (McCabe et al. 1997). In fact, the discovery of regulated cell death was first made in plants. The active self-elimination of wheat epidermal cells as a very efficient way to ward off intruding hyphae from the rust fungus *Puccinia* (Allen, 1923) was described decades before so called apoptosis became a buzz word in medicine. Given the numerous functions of regulated cell death, it comes as little surprise that this process can come in many forms that have stimulated a plethora of different names leading to considerable confusion and desperate attempts to regulate the terminological mess (Galluzzi et al., 2018; Locato and de Gara 2018). For the sake of clarity, we will refrain from delving too deeply into the ramifications of cell-death nomenclature, but pragmatically stick to the inducing factors. We will refer to those cases, where cells commit suicide as part of canonical development, as Programmed Cell Death (PCD). Typical examples would be the terminal differentiation of xylem cells, or the breakdown of the suspensor during late embryogenesis. Instead, so called Exogenously Induced Cell Death (EICD) ensues as active (and often adaptive) response to biotic or abiotic stress factors. Typical examples would be the Hypersensitive Reaction of resistant hosts to biotrophic pathogens (Gong et al., 2019), or the salt induced cell death of the root tip, which will stimulate the formation of lateral roots that will then scout the soil in the neighbourhood of the saline spot (Li et al., 2007).

Since plant cells are encased in a rigid cell wall, their breakdown shows cytological features that differ from apoptotic death of animal cells. This is also reflected on the molecular level, for instance by the absence of caspases, whose function is played by metacaspases and a couple of other proteases (for review see Piszczek and Gutman, 2007). Based on the behaviour of the vacuole, at least two types of regulated cell death can be discerned (for review see Lam, 2004). In developmental PCD, a combination of autophagy and release of hydrolases from the eventually collapsed vacuole remove the cell content (van Doorn, 2011), while during necrotic death occurring under severe abiotic stress, the

plasma membrane loses integrity during an early stage, which is followed by shrinkage of nuclei and protoplast. The hypersensitive response to biotrophic pathogens has also been called mixed type because it seems can express features of both necrosis and vacuolar cell death (van Doorn et al., 2011). Apoptotic degradation of animal cells is often linked with the formation of apoptotic bodies, whereby the cell is partitioned into smaller structures enveloped by plasma membrane sealing fragments of cytoplasm, nuclei, mitochondria, and the endomembrane system. Comparable structures have been observed in plant cells as well and might help to degrade and recycle proteins, or even parts of entire organelles, during plant development or environmental stress. Again, two types of autophagy have been described (van Doorn and Woltering, 2005): During so-called microautophagy, the tonoplast invaginates, such that cytoplasmic fractions are integrated into the vacuole. In contrast, during macroautophagy (reviewed in Bozhkov, 2018), a large phagophore is emerging from the endoplasmic reticulum and engulfs part of the cytoplasm, such that the content is surrounded by a double membrane. The outer membrane of this autophagosome can fuse with the tonoplast, such that the interior (still surrounded by the inner membrane) is released into the vacuole for degradation. The regulation of autophagosomes depends on autophagy-related (ATG) proteins, some of which, such as the ATG1/ATG13 act as kinases on protein substrates, while others, such as the phosphatidylinositol-3-kinase (PI3K) complex, convert phosphatidylinositol to phosphatidylinositol-3-phosphate (PI3P), seem to target to the membrane moiety.

To dissect the cellular details of regulated cell death and to link it with differential signal transduction requires a system, where cell death can be triggered by a signal. While this has been done extensively for the Hypersensitive Reaction, it is more difficult to address this for developmental PCD. Over the last decades, we have elaborated such a model. The cytokinin kinetin, widely known as a “hormone of life” for its stimulation of cell proliferation, can also act as “hormone of death” in particular situations. Seminal roots of *Vicia faba* ssp. *minor* respond to exogenous kinetin by PCD in their apical parts (Kunikowska et al. 2013; Doniak et al. 2016). This response is dependent on cellular differentiation, since it is absent in the meristematic cells, while parenchymatic cells of the root cortex initiate PCD within 2-3 days. The functional context may be linked to the formation of an aerenchyma, a tissue rich in intercellular spaces allowing oxygen to reach the metabolically active cells in the meristem, especially in dense soils, where diffusion is limiting.

Extensive research on this model case for developmental PCD revealed the following features: (i) formation of small, later larger acidic lytic vacuoles, (ii) condensation of heterochromatin at

concomitant decondensation of euchromatin, (iii) chromatin fragmentation mediated by exo-/endonucleolytic enzymes, (iv) sealing of plasmodesmata in the cell walls of living cortex cells bordering the aerenchymatic space linked with clogging by callose, (v) thickening of cell walls in the bordering non-dying cells, and (vi) formation of micronuclei and/or apoptotic-like (pseudoapoptotic) bodies (Kunikowska et al. 2013; Doniak et al. 2014; Kaźmierczak et al. 2017). On the cellular level this was accompanied by (a) reduction in the number of mitochondria and their morphological malformations due to excessive formation of reactive oxygen species (ROS) overproduction, (b) greater activity of catalases and superoxide dismutases ROS scavenging enzymes, and (c) increase in the total and cytosolic levels of Ca^{2+} ions in cortex cells (Doniak et al. 2016; Doniak et al. 2017) and a decrease in steady-state levels of ATP (Kaźmierczak and Soboska 2018). The molecular features of kinetin-induced cell death include (1) unaltered protein amount, (2) fluctuating activities of H_1- and core-histone kinases, (3) activation of serine- and cysteine-dependent proteases, as well as (4) changes in β1 proteasome subunit activity, (5) leakage of potassium ions from roots, (6) loss of plasma and ER membrane potentials (manifest as reduced content of unsaturated fatty acids in the ER), (7) malformations of the nuclear envelope, (8) reduced content of total lipids and lipid peroxides, (9) reduced amount of phospholipids and alterations of their composition, and (10) elevated amounts of cellulose, callose, and other cell wall bound sugars (Kunikowska et al. 2013; Doniak et al. 2014, Doniak et al. 2016; Doniak et al. 2017; Kaźmierczak et al. 2017).

This plethora of responses leads to the question, what is cause and what is consequence, requiring either a temporal sequence or spatial structuring. The Hypersensitive Response often initiates with the perception of pathogen effectors by specific nucleotide-binding-leucine-rich repeat (NB-LRR) receptors deriving from a co-evolutionary history of specific pathogens with their specific hosts (for review see Takken and Tameling 2009), activating specific members of metacaspases (Gong et al. 2019). For developmental PCD, perception and early signalling are not that clear. Perturbations in the integrity of the plasma membrane cause an activation of a NADPH oxidase. Respiratory burst oxidase homologue in the plasma-membrane, and consequent remodelling of cortical actin filaments can activate PCD (Eggenberger et al. 2017). For the regulated death of *Arabidopsis* cells in response to the cytokinin benzylaminopurine, the receptor CRE1/AHK4 is required (Vescovi et al. 2012). For tobacco BY-2 cells, phosphorylated cytokinins turned out to be active, which holds true both for isopentenyl adenosine (Mlejnek and Procházka 2002) and benzylaminopurine (Mlejnek et al. 2003). This ligand specificity indicates that also in this system a receptor triggers the process. While perception and signalling of developmental PCD and of HR seem to differ, certain downstream events linked with the

execution of cell death might be shared. For instance, caspase-like activities play a role also for cytokinin-induced cell death as to be concluded from inhibitor studies (Mlejnek and Procházka 2002). Likewise, intracellular burst, either originating from perturbation of mitochondrial (for review see Balint-Kurti 2019) or from plastid (for review see Ambastha et al. 2015) electron transport seems to be a common mechanism during the execution of both types of regulated cell death. This would mean that at some point the initially separate signal chains must converge. A possible candidate for such a merging hub would be the cytoskeleton. Although microtubules and actin filaments are functionally and structurally interconnecting and show significant remodelling during early phases of regulated cell death, they differ with respect to their primary response. Cortical actin, subtending the plasma membrane is rapidly depleted during HR (Chang et al. 2015), while the developmental PCD during vascular differentiation goes along with a specific bundling and elimination of cortical microtubules (Iakimova et al. 2017).

Aerenchymatic cells as well as vascular bundles differentiate from parenchymatic precursors and undergo terminal differentiation in response to specific plant hormones (aerenchyma in response to kinetin, vascular bundles in response to auxin). To observe the cellular details, especially the role of the cytoskeleton, is easier in a cell culture system. Cell suspensions of *Nicotiana tabacum* BY-2 (deriving from pith parenchyma that can generate aerenchyma and vasculature) can serve as convenient cellular model to study cell death in response to kinetin. We characterise this case of developmental PCD using histochemical approaches, including double staining with the membrane permeable dye Acridine Orange and the membrane-impermeable dye Ethidium Bromide, visualisation of cytosolic calcium ions, and detection of callose. Using marker lines expressing GFP fusions of β-tubulin or the actin-binding domain of fimbrin we also followed the cytoskeletal response to kinetin and can show that kinetin-induced cell death goes along with elimination of cortical microtubules, while actin filaments remain intact.

2 Materials and Methods

2.1 Cultivation of tobacco suspension cells

Different strains of tobacco BY-2 (*Nicotiana tabacum* L. cv Bright Yellow-2) suspension cells (Nagata et al. 1992) were used for this study. In addition to the non-transformed wild type, strain BY2-TuB6-GFP, expressing β-tubulin (AtTUB6) fused to GFP under the control of the constitutive Cauliflower Mosaic Virus 35S promotor (Hohenberger et al., 2011), and the strain GF11, expressing the second

actin-binding domain of fimbrin (AtFIM1) in fusion with GFP, also under a CaMV-35S promoter (Sano et al., 2005) were employed. Cells were subcultured in Murashige-Skoog medium at weekly intervals, by inoculating 1.5 ml of stationary culture cells into 30 ml of fresh medium and cultivated at 26°C in the dark under constant shaking an orbital shaker (IKA®KS 260 basic) as described previously (Maisch and Nick 2007).

2.2 Estimation of cell number over particular phases of the cell cycle

Frequency distributions over the different phases of the cell cycle were constructed for non-transformed wild type cells raised either under control conditions or in presence of 50 µM kinetin (Sigma-Aldrich, Deisenhofen, Germany) added at subcultivation. For this purpose, the nuclei were stained with 4', 6-diamidine-2'-phenylindole dihydrochloride **(**DAPI) according to Kaźmierczak (2010). In brief, the cells were fixed with 5% glutaraldehyde in 200 mM sodium phosphate buffer (pH 7.4, equal volume of cell suspension and fixative) for 1 h at room temperature. After that, cells could be stored at 4°C till the actual staining. For this purpose, the fixative was first washed out three times with three volumes of 100 mM sodium phosphate buffer (pH 7.4) and then three times (100 mM) with three volumes of staining buffer (100 mM sodium phosphate buffer supplemented with 10% of 200 mM citric acid). All washing steps were conducted in a custom-made staining chamber using a nylon mesh with a pore size of 10 µm (Nick et al. 2000). After the pre-equilibration, cells were stained with 2 µg ml^{-1} of DAPI in staining buffer for 15 min in the staining chamber inserted into small (5 ml) beakers before washing three times with three volumes of staining buffer void of DAPI. Aliquots of 50 µl of the stained cells where then viewed by fluorescence microscopy (Optiphot-2, Nikon, Japan) with UV2A filter, and photographed using ACT-1 digital camera (Precoptic, Poland). The fluorescence intensity of the nuclei reflecting the DNA content was quantified from the digital images using the ImageJ software (https://imagej.nih.gov). Hereby, the channels of the RGB image were split using the "split channel" tool. The red channel was then thresholded such that the nuclei were highlighted. Using the tracing tool, each nucleus was then individually selected to measure its integrated density. Subsequently, frequency distributions over fluorescence intensity were constructed, which allowed to infer the stage in the cell cycle (Kaźmierczak 2003): Hereby, cells in G_1 were estimated as proportion of cells with a fluorescence intensity below 100 a.u. added to half of those with intensities between 100 and 400 a.u., cells in S phase as proportion of cells with a fluorescence intensity between 400 a.u. and 600 a.u. divided by two, while the remaining cells were defined as being in G_2. Data represent mean and standard errors from two independent experiments consisting of three technical replications with a 600-800 individual nuclei per replication.

2.2 Estimation of cell mortality by the Evans Blue Dye Exclusion assay

To assess the effect of kinetin on mortality, non-transformed BY-2 wild type cells were followed over the entire cultivation cycle in response to 50 µM kinetin as compared to untreated cells. Mortality was scored by the Evans Blue Dye Exclusion Assay (Gaff and Okong' O-Ogola, 1971) as described in Sarheed et al. (2020). Data represent three independent replications with a population of 600 individual cells per replication.

2.3 Cytochemical characterisation by Acridin Orange / Ethidium Bromide staining

A double labelling with the membrane permeable dye Acridine Orange (100 µg mL^{-1}) and the impermeable dye Ethidium Bromide (100 µg mL^{-1}) in 200 mM Na phosphate buffer at pH 7.4 were used to get insight more cellular details on the type of kinetin induced mortality. Aliquots of 500 µl of cells cultivated under control conditions and cells cultivated in presence of 50 µM kinetin were collected daily from day 3 after subcultivation till the end of the cultivation cycle into a custom-made staining chamber and processed as described in Sarheed et al. (2020). Aliquots of 50 µl of the double-stained cells were then inspected by fluorescence microscopy (Diaplan, Leitz) using excitation in the blue (filter set I3, excitation 450-490 nm, beam splitter 510 nm, emission filter >515 nm). For each experimental set, around 350-400 cells were recorded by a digital camera (Leica DFC 500) controlled by a digital acquisition software (Leica Application Suite, v4). In this approach, the nuclei of cells with tight cell membranes will appear green, because they are exclusively labeled by Acridine Orange. With progressive permeabilisation of the membrane, the red signal from Ethidium Bromide will increase, such that the nuclei turn over orange into red. The resulting colours of the chromatin were quantified using the Scn Image quantitative image analysis software (https://scion-image.com) as described in Byczkowska et al. (2013). The resultant fluorescence intensity (RFI) allowed to classify the cells into different stages, exemplarily shown in Figure 3B: living cells appeared green, cells in dying stage I exhibited a yellow nucleus, whereby the nucleolus remained unstained, while cells in dying stage II were characterised by yellow nuclei where the nucleolus was labelled as well, and dead cells could be recognised by their red colour. Data represent mean and standard errors from two independent experiments consisting of three technical replications with a 350–400 individual cells per replication.

2.4 Quantification of callose

Callose was visualised and quantified using Aniline Blue (Kaźmierczak 2008). Cells were fixed in 2.5% glutaraldehyde in 200 mM sodium phosphate buffer (pH 7.4), and then pre-equilibrated three times for 3 min with 4 mM K_2HPO_4 (pH 9), prior to staining for 15 min with 0.05% (w/v) aniline blue

(Water Blue; Fluka) in 4 mM K_2HPO_4 (pH 9). Unbound dye was washed out thrice using the same buffer. Callose was then recorded by fluorescence microscopy (Optiphot-2, Nikon, Japan) upon excitation with short-wave blue-light (390–420 nm excitation filter as a green to yellow fluorescence. Digital images were recorded (ACT-1 digital camera, Precoptic, Poland) and the callose-dependent Aniline Blue signal quantified using the Scn Image quantitative image analysis software (https://scion-image.com) as described in (Kaźmierczak 2008). Data represent mean and standard errors from two independent experiments consisting of three technical replications with a 150–250 individual cells per replication.

2.5 Quantification of cytosolic calcium levels

Cytosolic calcium was estimated by chloro-tetracycline according to Doniak et al. (2016). After fixation in 2.5% glutaraldehyde in 200 mM sodium phosphate buffer (pH 7.4), the cells were washed three times for 5 min with 50 mM of staining buffer (Tris-HCl, pH 7.45) in the custom-made staining chamber. After draining, excess liquid was removed using with a filter paper, and the cells were stained for 5 min in 5-ml beakers with 100 μM chlorotetracycline in staining buffer. Unbound dye was washed out three times with staining buffer for 2 min and then cells were analysed by fluorescent microscopy (Optiphot-2, Nikon, Japan) recording digital images (ACT-1 digital camera, Precoptic, Poland) using filter set B2A. The green fluorescence was quantified using the Scn Image quantitative image analysis software (https://scion-image.com) as described in Kunikowska et al. (2013). Data represent mean and standard errors from two independent experiments consisting of three technical replications with 50 to 100 individual nuclei per replication.

2.6 Live-cell imaging of the cytoskeleton

We visualised microtubules by means of the *Arabidopsis thaliana β*-tubulin (*AtTuB6*) marker, carrying a N-terminal fusion with GFP (Hohenberger et al., 2011), and actin filaments by means of the second actin-binding domain of Arabidopsis thaliana fimbrin (*AtFIM1*) in fusion with GFP (Sano et al., 2005). We captured images by spinning-disc confocal microscopy using a CCD camera on an AxioObserver Z1 (Zeiss, Jena, Germany) through a 63 × LCI-Neofluar Imm Corr DIC objective (NA 1.3), exciting with the 488 nm emission line of an Ar-Kr laser and collecting the signals through a spinning-disc device (YOKOGAWA CSU-X1 5000). To operate, we used the ZEN 2012 (Blue edition) software platform and generated orthogonal projections from the recorded stacks, exporting the raw images as TIFF format. For each experimental set, representative images of at least three independent experimental series recording a population of 30 individual cells were selected.

2.7 Correlation analysis

We tested statistical significance for each trait individually using the Mann-Whitney *U* test and/or the Student's *t*-test (Microsoft Excel) using a threshold at $P \leq 0.05$. To detect correlations between two different traits x and y, we determined the respective Pearson correlation coefficient r_{xy} (Microsoft Excel). This coefficient varies between +1 and -1 depending on the direction of the correlation. When $|r_{xy}|$ was between 0.0 and 0.3, we considered this as lack of correlation, values between 0.3 and 0.8 indicated a moderate correlation, and values above 0.8 a strong correlation. Statistically, values above 0.3 are significant at $P < 0.05$. We visualised the result of this correlation analysis using yEd Graph Editor 3.20 (https://www.yworks.com/products/yed, open source).

3 Results

3.1 Kinetin induces arrest of the cell cycle and cell death in cycling cells of tobacco BY-2.

To get insight into the effect of kinetin on proliferating cells, 50 µM of kinetin were either added at time of subcultivation, or at the transition from cell proliferation to cell expansion. The nuclei were stained with DAPI, and mortality was scored by the Evans Blue Dye Exclusion Assay. Both readouts were followed over the entire cultivation cycle. In response to 50 µM kinetin administered at subcultivation, mortality remained low and equalled that seen in the untreated control (**Fig. 1A**). However, following day 3, mortality increased at a steady pace reaching 60% at the end of the cultivation cycle at day 7. In contrast, mortality in the untreated control remained low. When kinetin (again 50 µM) was added during the proliferation phase at day 3, the increase of mortality was correspondingly shifted to day 7. Since it is not possible to prolong the cultivation cycle beyond 7 days, because otherwise tobacco BY-2 undergo cell death, only the initial phase of this mortality response could be captured. The value seen at day 7 was exactly that seen at day 4, when kinetin was added at subcultivation. Thus, the time course was just shifted by 3 days. Thus, kinetin induces a cell death response that requires 3 days to become manifest. So, this cell death cannot be of an acute nature, but obviously requires cellular activities that require several days to proceed. To get insight into cellular aspects of the kinetin response, nuclei were stained with 4',6-diamidine-2'-phenylindole dihydrochloride (DAPI) at different time intervals after subcultivation, either in untreated controls, or in cells that had been treated with 50 µM kinetin from the time of subcultivation. When the cells were viewed at day 3 (around the peak of mitotic activity), the controls displayed large nuclei that were mostly located in the cell centre (**Fig. 1B**), characteristic for cells in G_2. In contrast, cells that had been

raised in presence of kinetin, showed distinctly smaller nuclei that were often located close to the cell wall, which is characteristic for cells in G_1. Two days later, at the peak of cell expansion, the nuclei in the kinetin-treated cells had increased in size and some were also seen in the cell centre, but still, they were significantly smaller than those of the control cells at this time point. Only at the end of the cultivation cycle, nuclear size in the kinetin-treated samples approached those of the control (**Suppl. Fig. S1**).

To corrobate the impression that kinetin arrests the cell cycle, we estimated the DAPI signals from the individual nuclei by quantitative image analysis (which allows to infer DNA content) and constructed frequency distributions over this inferred DNA content through the cultivation cycle (**Fig. 2**). For the untreated control at subcultivation (i.e., at day 0), most cells (60%) displayed a DNA content of 2C, indicating that they were in the G_1-phase of cell cycle (**Fig. 2A**). In contrast, cells in S-phase (2-4C) were less frequent (around 30%), and those with completed S-phase (4C) were even rarer (around 10%). At the time of maximal proliferation (between days 3 and 4), the incidence of cells in G_1-phase had dropped to around 40%, while cells during or after S-phase showed a concomitant increase (in the sum around 55%). During the subsequent phase of cell expansion, cells in G_1 accumulated to around 70%, while the frequency cells in S or G_2 dropped to a minimum (around 25% when cells with 2-4C and 4C are pooled). During the final phase of the cultivation cycle, more cells entered S-phase, such that the values for cells in G_1 dropped again to the initial level of around 60%. Thus, the dynamic fluctuation of DNA content per nucleus reflects a pattern, where cells enter a phase of rapid cycling that culminates between days 3 and 4. During the subsequent expansion phase, most cells remain arrested in G_1. During the end of the cultivation cycle, they move on into the S-phase, in anticipation of the next round of proliferations that are triggered by addition of fresh medium (which will also replenish cellular auxin levels).

The pattern observed for kinetin-treated cells was clearly different (**Fig. 2B**). During the first half of the cultivation cycle, the frequency of cells in G_1 (2C) dropped much sharper than in the control, and while increasing again after day 4, it did not return to the initial value of 60%, seen in the controls, but dropped again to around 20% at the end of the culture cycle. Instead, the initial increase of cells during S phase (2-4C), or with completed S phase (4C) increased more dramatically (in the sum reaching up to 80% at day 4, which is significantly higher than the around 55% found in the control). Although, the incidence of cells in S-phase dropped subsequently, overall, the cells remained at significantly higher levels in S-phase or G_2 as compared to the control. This was also reflected in a shift of the intensity

histogram towards higher intensities (**Suppl. Fig. S2**). These patterns support a scenario, where kinetin arrests the cell cycle in S-phase and, thus, represses cell division.

3.2 Cell death induced by kinetin shows cytological features of regulated cell death.

The cell death in response to kinetin might be of an unspecific quality, for instance, when the cellular processes activated by this hormone would exhaust vital functions of the cells. However, the resulting cell death might also be of a regulated nature. To differentiate between these two cases, we used a histochemical approach, staining the nuclei with two fluorescent dyes that differ with respect to membrane permeability. Acridine Orange is membrane permeable, while Ethidium Bromide is not. As long as the cell membranes are tight, the cells will appear green, while cells with a loss of membrane integrity will display nuclei that progressively change from orange into red. While most control cells appeared green even at day 7 of the cultivation cycle (**Fig. 3A**, upper row), kinetin treatment clearly increased the incidence of cells with red nuclei already from day 3 after subcultivation, indicative of a loss of membrane integrity (**Fig. 3A**, lower row). A closer look reveals that the transition from the cells with intact membrane integrity (green cells, classified as "alive") to those with a red nucleus (classified as dead) occurs through transitions, where both labels are present (**Fig. 3B**). These cells appear yellow. Most of these yellow cells, classified as "dying I", display yellow nuclei with unstained nucleoli (**Fig. 3B**, *nco*), a smaller fraction of these yellow cells, classified as "dying II", show yellow nuclei, where the nucleoli were lighting up massively as well. Obviously, in these cells, a permeability barrier still delineating the nucleolus during the stage "dying I", has broken down.

In the next step, we used this stageing system to quantify the cellular response to kinetin over time (**Fig. 4**). In the control, almost the entire population was alive, exclusively exhibiting the green signal from Acridine Orange (**Fig. 4A**). In contrast, for the cells cultivated in the presence of 50 µM kinetin, the frequency of this class decreased progressively to less than 40% at day 7 (**Fig. 4B**). Concomitantly, the frequency of cells in stage "dying I" increased steadily, and even exceeded that of living cells at the end of the culture cycle. From days 3 and 4, also a minor fraction of cells in stage "dying II" (up to 15% at day 7) appeared. Interestingly, the frequency of dead cells remained low (below 5%) even at the end of the culture cycle. This indicates that dead cells are quickly degraded, such that their steady-state level remains low.

3.3 Intracellular calcium levels are elevated in response to kinetin.

Regulated cell death in plants is often heralded by an increase of cytosolic calcium levels (reviewed in Huysmans et al. 2017). For instance, an increase of calcium is driving the activation of metacaspases executing autolysis in *Arabidopsis* (Watanabe and Lam 2011). We visualised, therefore, intracellular calcium using chloro-tetracycline through the entire cultivation cycle (**Suppl. Fig. S3**). In proliferating control cells, at day 3 after subcultivation, calcium was found in cytoplasmic strands, the nucleus, and close to the cell walls, especially in the cross-walls, where neighbouring cells are interconnected by plasmodesmata (**Fig. 5A**, upper row). Later, at day 7 after subcultivation, the signal condensed to the nucleus, such that cytoplasm and cell walls were depleted from the signal. In response to kinetin, the fluorescence was significantly increased, not only in proliferating cells, but also still in the stationary cells (**Fig. 5A**, lower row). This impression was confirmed by the quantification (**Fig. 5B**). Already from day 2, the calcium signal in kinetin-treated cells increased drastically to around twice the level seen in the control, and while the signal gradually dissipated over time in both cases, this twofold elevation persisted till the end of the cultivation cycle. Thus, kinetin induces a strong and persistent increase of intracellular calcium levels.

3.4 Kinetin is suppressing the accumulation of callose at the cross walls.

Plasmodesmata are crucial for cell-cell communication in plants and in our previous work on kinetin-induced cell death of root cells (Doniak et al. 2017), we had observed that those cells that survived, had deposited higher levels of callose at the plasmodesmata. This led us to visualise callose by Aniline Blue in tobacco BY-2 cells and to follow the signal over time in control cells and in cells treated with 50 µM of kinetin (**Fig. 6**). In control cells, the callose signal increased strongly, by a factor of more than fourfold till the end of the proliferation phase (day 4 after subcultivation and then dropped back swiftly to almost the initial level within one day. In the kinetin-treated cells, the increase was delayed and strongly dampened. This increase initiated only at day 3 and reached a plateau of around two-fold at day 4 but was then sustained. As a result, the callose levels were higher in the kinetin-treated cells from day 6, because at that time the control cells had already returned to the initial (lower) level. The sharp peak of callose accumulation in proliferating control cells and the clear suppression and delay of this peak in cells treated with kinetin reflects the arrested cell cycles seen for the time course of DNA content (**Fig. 2**).

3.5 Correlation analysis supports a central role of calcium and callose deposition.

To facilitate identification of correlative patterns, we conducted a systematic analysis of Pearson correlation coefficients between all quantitative readouts, using a threshold of $P < 0.05$, correlating to a Pearson correlation coefficient above 0.3. The global correlation network (**Fig. 7A**) is placing cytosolic calcium ions and callose into the centre of the network. Within this network, two functional contexts emerge. On the one hand, the frequency of living, dead, hypoploid (C < 2 n) and diploid cells correlates positively with calcium levels (**Fig. 7B**), while the amount of callose, the frequency of cells in stage-I of dying at the first step and the frequency of S-phase correlates negatively (**Fig. 7B**). The second functional network derives from the positive correlation of cells at C = 4 n and of dead cells with calcium levels, while callose, the frequency of cells in stage-I of dying, and cells in S-phase correlate negatively (**Fig. 7C**). Thus, calcium and callose change correlate inversely.

3.6 Kinesin specifically disrupts microtubules and perturbs cell axiality.

The cytoskeleton has been discussed to respond to signals that induce programmed cell death, whereby actin filaments are often linked with defence-related hypersensitive cell death (Chang et al., 2015), while microtubular reorganisation or disruption is characteristic for developmentally induced forms of cell death, such as the formation of xylem vessels (Iakimova et al., 2017). We followed, therefore, the response of microtubules in the tobacco BY-2 marker line TuB6-GFP (Hohenberger et al., 2011) to a treatment with kinetin. At proliferation phase, the controls formed axial files of dividing cells that exhibited fine, but not aligned cortical microtubules (**Fig. 8A**) and a radial array of trans-vacuolar microtubules emanating from the nucleus (**Fig. 8B**). This microtubule array is characteristic for cells in G2. Cells that had faced kinetin treatment (**Fig. 8C**) had lost this axiality, both with respect to the individual cell shape (that did not reveal any axiality) as well as with respect to the alignment of individual cells. Instead of the axially aligned cell file, cells were forming disordered, triangular clusters. Instead of the delicate microtubule arrays prevalent in the controls, only single microtubules were present and those did not form any organised structures. We noticed a strong diffuse background in the cytoplasm, probably deriving from non-assembled tubulin heterodimers tagged by GFP. At the stage of cell expansion, control cells displayed an array of cortical microtubules aligned perpendicular to the expansion phase (**Fig. 8D**), while the radial microtubules tethering the nucleus had started to fade somewhat as compared to the proliferating cells (compare **Fig. 8D** to **8B**). This pattern is expected from cells that proceed through G_1. In case of kinetin treatment (**Fig. 8E**), there was no expansion axis

to be discerned, and instead of cortical microtubules, we observed numerous punctate structures that were dispersed all over the cytoplasm and might represent cortical nucleation sites.

As to find out, whether the effect of kinetin was specific for microtubules, or whether it originated from a general breakdown of the cytoskeleton, we also probed actin filaments, using the tobacco BY-2 marker line GF11 (Sano et al., 2005) expressing the actin-binding domain 2 from plant fimbrin in fusion with GFP (FABD2-GFP). In proliferating cells, kinetin caused a certain bundling of cortical actin filaments and trans-vacuolar actin cables became more prominent, as compared to the control (**Figs. 9A, B**). The same phenomenon was observed in expanding cells (**Figs. 9C, D**). However, in contrast to microtubules, actin filaments remained completely intact, we did not note any indication for a disruption or elimination. Thus, the cytoskeletal effect of kinetin is specific for microtubules.

4 Discussion

The motivation behind the current study was to get insight into the cellular mechanism of kinetin-induced cell death, a developmental form of PCD that was first observed in cortex cells of *Vicia faba* spp. *minor* seminal roots (Kunikowska et al. 2013; Doniak et al. 2014). We transferred this phenomenon to tobacco BY-2 cells, mainly for two reasons. First, tobacco BY-2 shows vigorous cell proliferation, while maintaining a residual, but controlled sequence of cell states as prerequisite for quantitative phenotyping (Huang et al., 2017). Second, this cell line is amenable to transformation, such that GFP-tagged strains allow for life-cell imaging. In the current work, we first show that kinetin-induced PCD can be recapitulated in tobacco BY-2 cells. This PCD in response to kinetin correlates with an arrest of the cell cycle, deregulation of DNA replication, increase of cytosolic calcium, suppression of callose deposition, and a complete loss of microtubule integrity, which is followed by a complete loss of cell axiality. These findings lead to a couple of questions. First, does the kinetin response meet criteria for a developmental PCD? Second, what can we deduce from the correlative network connecting the different features of this phenomenon? Third, what might be the role of the cytoskeleton in the elicitation or execution of PCD? These considerations culminate in a working model, where kinetin, mediated by calcium, causes the breakdown of the microtubule network, which, either by release of executing proteins, or by mitotic catastrophe, will result in PCD. We will conclude by developing some ideas to test implications of this model in future work.

4.1 The response to kinetin meets hallmarks of a developmental PCD.

The response of BY-2 cells to kinetin meets several criteria of a developmental PCD. First, several days are required until the death response becomes manifest, which is not compatible with acute toxicity. Second, by double staining with Acridine Orange and Ethidium Bromide we can follow the loss of plasma-membrane integrity and the permeabilisation of the nuclear envelope (**Fig. 3**). Interestingly, the fraction of cells, where also the nucleolus breaks down (stage II of dying) is negligible, indicating that the karyoplasm still maintains its structure till the end. This would not be expected, if the cells were dying in an acute and unregulated way. The progressive disintegration of cellular membranes, not as unspecific consequence of cellular breakdown, but as upstream event, belongs to the main hallmarks of regulated cell death (van Doorn 2011; van Doorn et al. 2011; Doniak et al. 2014; Kaźmierczak et al. 2017; Galluzzi et al. 2018). A further hallmark of regulated cell death is the link with aberrant cell cycling. Our quantifications of nuclear DNA content (**Fig. 2**) suggest that kinetin arrests the cell cycle in the S-phase. As a response preceding the arrest of the cell cycle and the loss of membrane integrity, we observed a drastic increase in cytosolic calcium (**Fig. 5**), which seems to transduce the kinetin signal upon cellular responses.

Our observation that calcium levels become elevated during cytokinin-dependent cell death is consistent with findings in tobacco BY-2 cells, where inhibition of calcium influx by different inhibitors mitigated cell death in response to hydrogen peroxide (Bobal et al. 2015). Conversely, the development of leaf perforations in the lace plant, a unique system to study developmental PCD, was promoted by the calcium ionophore A23187 and inhibited by the calcium channel inhibitor Ruthenium Red (Fraser et al. 2020). Using the lysogenic formation of oil cavities in *Citrus* as model, the activating role of calcium could be linked to the activation of calcium-dependent nucleases (Bai et al. 2020).

This increase in calcium is accompanied by a suppression of callose deposition that, in control cells, accompanies cell proliferation (**Fig. 6**). The antagonistic relationship between calcium and callose observed in our study (**Fig. 7C**) is consistent with observations in the identification of a mutant in *Arabidopsis thaliana* which is overly sensitive to low calcium and functionally null for callose synthesis (Shikanai et al. 2020). Conversely, our previous finding (Doniak et al. 2017) that those root cortex cells in *Vicia faba ssp. minor* that did not respond to kinetin by PCD showed increased callose deposition at their plasmodesmata.

Thus, the kinetin response of tobacco BY-2 cells to exogenous kinetin displays several very specific features of developmental PCD and it even preserves details of the functional context between these features, such as the antagonistic behaviour of cytosolic calcium and callose deposition. It is therefore straightforward and justified to describe this phenomenon as regulated PCD. Our data are in line with previous results (Mlejnek and Procházka 2002), where cell death in BY-2 in response to the cytokinin isopentenyl adenosine was mitigated by inhibitors of caspase activity.

4.2. What is the functional context of calcium, callose and cell cycle?

Calcium influx has been demonstrated for numerous cytokinin responses starting from the classical work in mosses, where this phenomenon is integrated into the formative asymmetric division of caulonema cells required to define a bud (Saunders et al. 1983). Cytokinins can deploy a histidine-kinase dependent two-component system (for a classical review see Hutchison and Kieber 2002). Using suspension cell cultures derived from respective mutants, the receptor HK4 was found to be central for cytokinin induced PCD (Vescovi et al. 2012). Generally, cytokinin receptors deploy signalling through mobile response regulators, and some of those connect with G-protein signalling (Wang et al. 2017), which also would explain findings, where overexpression of a trimeric G-protein leads to a higher sensitivity against cytokinins (Plakidou-Dymock et al. 1998). G-protein coupled receptors are well known to induce calcium influx (for review see Tuteja and Sopory 2008), especially in stress-related contexts, such as the membrane transducer COLD1 driving cold sensing in rice (Ma et al. 2015). A straightforward working model would place the increase in cytosolic calcium observed in the current study (**Fig. 5**), as well as in studies on kinetin-induced cell death in roots (Doniak et al. 2016, 2017) downstream of cytokinin triggered activation of G-protein signalling. A testable implication of this model would be that treatment with pertussis toxin should suppress the kinetin response.

The induction of cytosolic calcium will activate ethylene synthesis. The mechanism seems to run through activation of calcium dependent protein kinases CPK16 (Huang et al. 2013) which phosphorylates ACC synthase at specific serine residues, such that it will remain protected from proteolytic decay. As a result, this enzyme will synthetise more of the direct ethylene precursor 1-aminocyclopropane-1-carboxylic acid (ACC). In fact, cytokinin treatment has been shown to increase the stability of this enzyme (Chae et al., 2003). Ethylene is a central activator of PCD (for review see Wojciechowska et al. 2018) and has been specifically detected as crucial factor in cytokinin induced developmental cell death (Doniak et al. 2017).

We observe a negative correlation between calcium ions and callose abundance. This *β*-glucan (*β*-1,3-glucose polymer) is often discussed in the context of pathogen defence and seems to be a tool to establish and maintain borders (Jacobs et al. 2003). Analysis of the *massue* mutant in *Arabidopsis thaliana* led to the discovery that callose is required for cytokinesis and represents the major luminal polymer in the cell plate, although it is replaced by cellulose, xyloglucans and pectins in the maturating cell wall (Thiele et al. 2009) but persists around the plasmodesmata (Wu et al. 2018). The synthesis of callose to delineate borders, might have been an acquisition of the ancestral line within the pteridophytes that gave rise to the seed plants (Drábková and Honys, 2017), but pre-cursor might be even older, because the functional link between callose and cytokinesis is also present in the Zygnematophyceae, a sister clade of the terrestrial plant lineage (Davis et al. 2020). Microtubules might be the missing link between elevated calcium, suppressed callose deposition and block of the cell cycle, because microtubule can be eliminated through modulation of calcium- and calmodulin-binding associated proteins (Kölling et al. 2019). Elimination of microtubules in response to calcium would culminate in disrupted cytokinesis and should lead to bi- or even multinuclear cells. However, it would not explain the observed suppression of endoreplication in response to cytokinins. This indicates that the suppression of callose is not upstream of microtubule elimination, but rather is parallel phenomenon triggered by a common cause (increase of cytosolic calcium).

Kinetin was originally discovered by its effect of mitosis, using plant cells (onion root tips) as model (Guttman 1956). The mitotic stimulation is caused by inducing the progression through the G_2-M checkpoint through activation of a tyrosine kinase that phosphorylates the $p34^{cdc2}$ histone 1 kinase, which as a result becomes inhibited (tobacco cells, Zhang et al. 1996). In animal cells, mitotic arrest is often followed by apoptotic cell death (for reviews see Castedo et al. 2004, Kastan and Bartek 2004), and important anti-cancer compounds such as paclitaxel (Jordan et al. 1996) act through inducing this so-called mitotic catastrophe, often linked with multipolar spindles (Roninson et al. 2001). Often, cancer cells circumvent this bottle neck by centriole clustering. Plant compounds such as gallic acid that can block this clustering, can specifically interfere with the proliferation of cancer cells (Tan et al. 2015). To what extent mitotic catastrophe exists in plants, is unclear. In a previous study, we have observed in tobacco BY-2 cells that cadmium can cause a death response displaying apoptotic features such as DNA laddering, if administered at the G_2-M transition, while cells in G_1 are dying in a necrotic fashion (Kuthanová et al. 2008). This would indicate that death in response to mitotic arrest also occurs in plants. Our finding that the cell death in response to kinetin is accompanied by an increased

frequency of nuclei with lower DNA content would be consistent with a scenario, where the cell cycle is suppressed, which would then be followed by cell death.

In animal cells, apoptotic death in response to mitotic arrest is characterised by the activation of caspase-2, cytochrome c, and the p53 protein. In addition, a caspase-independent mechanism uses the activation of endonuclease G, followed by DNA fragmentation (Castedo et al. 2004). The decrease of p53 levels can be circumvented by endoreplication, which allows DNA repair and exit from apoptosis, but this works only, if the G_2-M checkpoint has not been reached (Castedo et al. 2004). A link between kinetin and DNA damage has been proposed for the cortex cell of faba bean seedling roots (Doniak et al. 2014; Kaźmierczak and Soboska 2018). Moreover, kinetin can be form product from DNA oxidation *in vivo* (Barciszewski et al. 1997) and, thus, might act as signal reporting for DNA damage, initiating cell death to prevent damaged cells from proliferating.

4.3 Microtubules versus actin: does the cytoskeleton decide the type of death?

The thorough elimination of microtubules followed by a complete loss of cell axiality (**Fig. 8**) belongs to the most striking cellular kinetin responses observed during the current study. This microtubule elimination is not an unspecific consequence of ensuing cell death, because at the same time, actin filaments as second important component of the cytoskeleton remains intact (**Fig. 9**). This delineates kinetin-induced cell death from defence-related cell death, where subcortical actin subtending the plasma membrane is rapidly degraded (Chang et al. 2015). Does this mean that the two ways to die use different components of the cytoskeleton as weapon to execute cell death?

Our observation stimulates three questions: 1. How can kinetin cause microtubule elimination? 2. How is microtubule elimination causally linked with cell death? 3. Which upstream event decides upon the cytoskeletal target to be dismantled?

The elimination of microtubules might well a consequence of the elevated calcium levels induced by kinetin (**Fig. 5**). A straightforward hypothesis would imply that calmodulin-related proteins (for review see Kölling et al. 2019) modulate the activity of microtubule-associated proteins. In fact, several members of the IQD clade of calmodulin-binding proteins have been shown to convey calcium triggered subdomains to microtubules (Bürstenbinder et al. 2017). The resulting breakdown of the microtubular cytoskeleton would then lead to mitotic catastrophe and deploy cell death. Alternatively, calcium might activate metacaspases (Zhu et al. 2020) that could break down microtubule-associated

proteins – in analogy to the breakdown of neural MAP τ by caspase 3 (Fasulo et al. 2000). Likewise, a direct breakdown of microtubules is conceivable as shown for apoptosis triggered by caspase 8 (Mielgo et al. 2009). While the breakdown of the microtubular cytoskeleton seems to be linked with calcium, the situation is different for actin filaments. Here, it is the membrane located NADPH oxidase Respiratory burst oxidase Homologue that is responsible for the breakdown of the cortical actin network (Chang et al. 2015). Both, apoplastic oxidative burst and calcium influx, are important signals conveying information about different stress conditions. They can occur with different timing and balance and this temporal signature has been shown to activate different qualities of defence responses in grapevine cells (Chang and Nick 2012). It is, therefore, worth to address the function of the cytoskeleton in kinetin-induced cell death using inhibitors blocking calcium influx, apoplastic oxidative burst, and the two components of the cytoskeleton, actin filaments and microtubules. The possibilities outlined above can be used to infer testable implications and get deeper insight into the role of the cytoskeleton for steering cell death. It will also be rewarding to use tobacco cell lines, where specific classes of metacaspases have been overexpressed to dissect the molecular mechanism behind this phenomenon.

Acknowledgements

This work was supported by the University of Łódź to AK (No. 1409) to AK. Technical assistance of Sabine Purper is gratefully acknowledged.

References

Allen RF (1923) A cytological study of infection of Baart and Kanred wheats by *Puccinia graminis tritici*. J Agricult Res 23:131–152.

Ambastha V, Tripathy BC, Tiwari BS (2015) Programmed cell death in plants: A chloroplastic connection. Plant Signaling Behavior 10:e989752. doi 10.4161/15592324.2014.989752

Bai M, Liang MJ, Huai B, Gao H, Tong PP, Shen RX, He HJ, Wu H (2020) Ca^{2+}-dependent nuclease is involved in DNA degradation during the formation of the secretory cavity by programmed cell death in fruit of *Citrus grandis* 'Tomentosa'. J Exp Bot 71:4812–4827. doi 10.1093/jxb/eraa199

Balint- Kurti P (2019) The plant hypersensitive response: concepts, control and consequences. Mol Plant Pathol 20:1163–1178. doi 10.1111/mpp.12821

Barciszewski J, Siboska GE, Pedersen BO, Clark BF, Rattan SI (1997) A mechanism for the in vivo formation of N_6-furfuryladenine, kinetin, as a secondary oxidative damage product of DNA. FEBS Lett 414:457–460. doi 10.1016/s0014-5793(97)01037-5

Bobal P, Otevrel J, Poborilova Z, Vaverková V, Csollei J, Babula P (2015) Application of BY-2 cell model in evaluating an effect of newly prepared potential calcium channel blockers. Pak J Pharm Sci 28:1281–1293.

Bozhkov PV (2018) Plant autophagy: mechanisms and functions. J Exp Bot 69:1281–1285. doi 10.1093/jxb/ery070

Byczkowska A, Kunikowska A, Kaźmierczak A (2013) Determination of ACC-induced cell-programmed death in roots of *Vicia faba ssp. minor* seedlings by acridine orange and ethidium bromide staining. Protoplasma. 250:121–128. doi 10.1007/s00709-012-0383-9

Bürstenbinder K, Möller B, Plötner R, Stamm G, Hause G, Mitra D, Abel S (2017) The IQD Family of Calmodulin-Binding Proteins Links Calcium Signaling to Microtubules, Membrane Subdomains, and the Nucleus. Plant Physiol 173:1692–1708. doi 10.1104/pp.16.01743

Castedo M, Perfettini JL, Roumier T, Andreau K, Medema R, Kroemer G (2004) Cell death by mitotic catastrophe: a molecular definition. Oncogene 23:2825–2837. doi 10.1038/sj.onc.1207528

Chae HS, Faure F, Kieber JJ (2003) The *eto1*, *eto2*, and *eto3* mutations and cytokinin treatment increase ethylene biosynthesis in *Arabidopsis* by increasing the stability of ACS protein. Plant Cell 15:545–559. doi 10.1105/tpc.006882

Chang X, Nick P (2012) Defence Signalling Triggered by Flg22 and Harpin Is Integrated into a Different Stilbene Output in Vitis Cells. PLoS ONE 7:e40446. doi 10.1371/journal.pone.0040446

Chang X, Riemann M, Nick P (2015) Actin as deathly switch? How auxin can suppress cell-death related defence. PloS ONE 10:e0125498. doi 10.1371/journal.pone.0125498

Davis DJ, Wang M, Sørensen I, Rose JKC, Domozych DS, Drakakaki G (2020) Callose deposition is essential for the completion of cytokinesis in the unicellular alga *Penium margaritaceum*. J Cell Sci 133:jcs249599. doi 10.1242/jcs.249599

Doniak M, Barciszewska MZ, Kaźmierczak J, Kaźmierczak A (2014) The crucial elements of the 'last step' of programmed cell death induced by kinetin in root cortex of *V. faba ssp. minor* seedlings. Plant Cell Rep 33:2063–2067. doi 10.1007/s00299-014-1681-9

Doniak M, Byczkowska A, Kaźmierczak A (2016) Kinetin-induced programmed death of cortex cells is mediated by ethylene and calcium ions in roots of *Vicia faba ssp. minor*. Plant Growth Reg 78:335–343. doi 10.1007/s00709-012-0466-7

Doniak M, Kaźmierczak A, Byczkowska A, Glińska S (2017) Reactive oxygen species and sugars may be the messengers in kinetin-induced death of root cortex cells of *V. faba ssp. minor* seedlings. Biol. Plant. 61:178–186. doi 10.1007/s00709-012-0466-7

Drábková ZL, Honys D (2017) Evolutionary history of callose synthases in terrestrial plants with emphasis on proteins involved in male gametophyte development. PLoS ONE 12:e0187331. doi 10.1371/journal.pone.0187331

Eggenberger K, Sanyal P, Hundt S, Wadhwani P, Ulrich AS, Nick P (2017) Challenge integrity: The cell-permeating peptide BP100 interferes with the actin-auxin oscillator. Plant Cell Physiol 58:7 –85. doi 10.1093/pcp/pcw161.

Fasulo L, Ugolini G, Visintin M, Bradbury A, Brancolini C, Verzillo V, Novak M, Cattaneo A (2000) The neuronal microtubule-associated protein tau is a substrate for caspase-3 and an effector of apoptosis. J Neurochem 75:624–633. doi 10.1046/j.1471-4159.2000.0750624.x

Fraser MS, Dauphinee AN, Gunawardena AHLAN (2020) Determining the effect of calcium on cell death rate and perforation formation during leaf development in the novel model system, the lace plant (*Aponogeton madagascariensis*). J Microsc 278:132–144. doi 10.1111/jmi.12859

Gaff DF, Okong'o-Ogola O (1971) The use of non-permeating pigments for testing the survival of cells. J Exp Bot 22:756–758. doi 10.1093/jxb/22.3.756

Galluzzi L, Vitale I et al (2018) Molecular mechanisms of cell death: recommendations of the Nomenclature Committee on Cell Death 2018. Cell Death Differ. 25:486–541. doi 10.1038/s41418-017-0012-4

Gong P, Riemann M, Stöffler N, Dong D, Gross B, Markel A, Nick P (2019) Two grapevine metacaspase genes mediate ETI-like cell death in grapevine defence against infection of *Plasmopara viticola*. Protoplasma 256:951–969. doi 10.1007/s00709-019-01353-7

Guttman R (1956) Effects of kinetin on cell division, with special reference to initiation and duration of mitosis. Chromosoma 8:341–350. doi 10.1007/BF01259506

Hohenberger P, Eing C, Straessner R, Durst S, Frey W, Nick P (2011) Plant Actin Controls Membrane Permeability. BBA Membranes 1808:2304–2312. doi 10.1016/j.bbamem.2011.05.019

Huang SJ, Chang CL, Wang PH, Tsai MC, Hsu PH, Chang IF (2013) A type III ACC synthase, ACS7, is involved in root gravitropism in Arabidopsis thaliana. J Exp Bot 64:4343–4360. doi 10.1093/jxb/ert241

Huang X, Maisch J, Nick P (2017) Sensory role of actin in auxin-dependent responses of tobacco BY-2. J Plant Physiol 218:6–15. doi 10.1016/j.jplph.2017.07.011

Hutchison CE, Kieber JJ (2002) Cytokinin Signaling in Arabidopsis. The Plant Cell Supplement S47–S59. doi 10.1105/tpc.010444

Huysmans M, Lema AS, Coll NS, Nowack MK (2017) Dying two deaths – programmed cell death regulation in development and disease. Curr Opin Plant Biol 35:37–44. doi 10.1016/j.pbi.2016.11.005

Iakimova ET, Woltering EJ (2017) Xylogenesis in zinnia (*Zinnia elegans*) cell cultures: unravelling the regulatory steps in a complex developmental programmed cell death event. Planta 245:681–705. doi 10.1007/s00425-017-2656-1

Jacobs AK, Lipka V, Burton RA, Panstruga R, Strizhov N, Schulze-Lefert P, Finchera GB (2003) An Arabidopsis callose synthase, GSL5, is required for wound and papillary callose formation. Plant Cell 15:2503–2513. doi 10.1105/tpc.016097

Jordan MA, Wendell K, Gardiner S, Derry WB, Copp H, Wilson L (1996) Mitotic block induced in HeLa cells by low concentrations of paclitaxel (Taxol) results in abnormal mitotic exit and apoptotic cell death. Cancer Res 56:816–825.

Kastan MB, Bartek J (2004) Cell-cycle checkpoints and cancer. Nature 432:316–323. doi 10.1038/nature03097

Kaźmierczak A (2003) Endoreplication in *Anemia phyllitidis* coincides with the development of gametophytes and male sex. Physiol Plant 138:321–328. doi 10.1111/j.1399-3054.2009.01323.x

Kaźmierczak A (2008) Cell number, cell growth, antheridiogenesis, and callose amount is reduced and atrophy induced by deoxyglucose in *Anemia phyllitidis* gametophytes. Plant Cell Rep 27, 381–382. doi 10.1007/s00299-007-0501-x

Kaźmierczak A (2010) Endoreplication in *Anemia phyllitidis* coincides with the development of gametophytes and male sex. Physiol Plant 138, 321–328. doi 10.1111/j.1399-3054.2009.01323.x

Kaźmierczak A, Doniak M, Bernat P (2017) Membrane-related hallmarks of kinetin-induced PCD of root cortex cells. Plant Cell Rep. 36, 343–353. doi 10.1007/s00299-016-2085-9

Kaźmierczak A, Soboska K (2018) Fate of nuclear material during subsequent steps of the kinetin-induced PCD in apical parts of *Vicia faba ssp. minor* seedling roots. Micron 110, 79–87. doi 10.1016/j.micron.2018.04.009

Kölling M, Kumari P, Bürstenbinder K (2019) Calcium- and calmodulin-regulated microtubule-associated proteins as signal-integration hubs at the plasma membrane–cytoskeleton nexus. J Exp Bot 70, 387–396. doi 10.1093/jxb/ery397

Kunikowska A, Byczkowska A, Kaźmierczak A (2013) Kinetin induces cell death in root cortex cells of *Vicia faba ssp. minor* seedlings. Protoplasma 250, 851–861. doi 10.1007/s00709-012-0466-7

Kuthanová A, Fischer L, Nick P, Opatrný Z (2008) Cell cycle phase-specific death response of tobacco BY-2 cell line to cadmium treatment. Plant Cell Environment 31, 1634-1643. doi 10.1111/j.1365-3040.2008.01876.x

Lam E (2004) Controlled cell death, plant survival and development. Nature Reviews Molecular Cell Biology 5, 305–315. doi 10.1038/nrm1358

Li J-Y, Jiang A-L, Zhang W (2007) Salt stress-induced programmed cell death in rice root tip cells. Journal of Integrative Plant Biology 49, 481–486. doi 10.1111/j.1744-7909.2007.00445.x

Locato V, de Gara L (2018) Programmed Cell Death in Plants: An Overview. *Methods in Molecular Biology* **1743**, 1–7. doi 10.1007/978-1-4939-7668-3_1

Ma Y, Dai XY, Xu YY, et al. 2015. COLD1 confers chilling tolerance in rice. Cell 160, 1209–1221. doi 10.1016/j.cell.2015.01.046

Maisch J, Nick P (2007) Actin is involved in auxin-dependent patterning. Plant Physiol 143, 1695–1704. doi 10.1104/pp.106.094052

McCabe PF, Valentine TA, Forsberg S, Pennella R (1997) Soluble Signals from Cells Identified at the Cell Wall Establish a Developmental Pathway in Carrot. The Plant Cell 9, 2225–2241. doi 10.1105/tpc.9.12.2225

Mielgo A, Torres V, Clair K et al (2009) Paclitaxel promotes a caspase 8-mediated apoptosis through death effector domain association with microtubules. Oncogene 28, 3551–3562. doi 10.1038/onc.2009.210

Mlejnek P, Doležel P, Procházka S (2003) Intracellular phosphorylation of benzyladenosine is related to apoptosis induction in tobacco BY-2 cells. Plant Cell Environ 26, 1723–1735. doi 10.1046/j.1365-3040.2003.01090.x

Mlejnek P, Procházka S (2002) Activation of caspase-like proteases and induction of apoptosis by isopentenyladenosine in tobacco BY-2 cells. Planta 215, 158–166. doi 10.1007/s00425-002-0733-5

Nagata T, Nemoto Y, Hasezawa S (1992) Tobacco BY-2 cell line as the “Hela” cell in the cell biology of higher plants. Int Rev Cytol 132, 1–30. doi 10.1016/S0074-7696(08)62452-3

Nick P, Heuing A, Ehmann B (2000) Plant chaperonins: a role in microtubule-dependent wall-formation? Protoplasma 211, 234–244. doi 10.1007/BF01304491

Piszczek E, Gutman W (2007) Caspase-like proteases and their role in programmed cell death in plants. Acta Physiol Plant 29, 391–398. doi 10.1007/s11738-007-0086-6

Plakidou-Dymock S, Dymock D, Hooley R (1998) A higher plant seven-transmembrane receptor that influences sensitivity to cytokinins. Curr Biol 6, 315–324. doi 10.1016/S0960-9822(98)70131-9

Roninson IB, Broude EV, Chang B-D 2001. If not apoptosis, then what? Treatment-induced senescence and mitotic catastrophe in tumor cells. Drug Resist Updat 4, 303–313. doi 10.1054/drup.2001.0213

Sano T, Higaki T, Oda Y, Hayashi T, Hasezawa S (2005) Appearance of actin microfilament 'twin peaks' in mitosis and their function in cell plate formation, as visualized in tobacco BY-2 cells expressing GFP–fimbrin. Plant Journal 44, 595–605. doi 10.1111/j.1365-313X.2005.02558.x

Sarheed MM, Rajabi F, Kunert M, Boland W, Wetters S, Miadowitz K, Kaźmierczak A, Sahi VP, Nick P (2020) Cellular Base of Mint Allelopathy: Menthone Affects Plant Microtubules. Front Plant Sci 11:546345. doi 10.3389/fpls.2020.546345

Saunders MJ, Hepler PK (1983) Calcium antagonists and calmodulin inhibitors block cytokinin-induced bud formation in *Funaria*. Dev Biol 99:41–49. doi 10.1016/0012-1606(83)90252-x

Shikanai Y, Yoshida R, Hirano T, Enomoto Y, Li BH, Asada M, Yamagami M, Yamaguchi K, Shigenobu Sh, Tabata R, Sawa SI, Okada H, Ohya Y, Kamiya T, Fujiwara T (2020) Callose Synthesis Suppresses Cell Death Induced by Low-Calcium Conditions in Leaves. Plant Physiol 182:2199–2212. doi 10.1104/pp.19.00784

Takken FL, Tameling WI. 2009. To nibble at plant resistance proteins. Science 324, 744–746. doi 10.1126/science.1171666

Tan S, Grün C, Guan X, Zhou Z, Schepers U, Nick P (2015) Gallic acid induces mitotic catastrophe and inhibits centrosomal clustering in HeLa cells. J Toxicol in vitro 30, 506–513. doi 10.1016/j.tiv.2015.09.011

Tanouchi Y, Lee AJ, Meredith H, You L (2013) Programmed cell death in bacteria and implications for antibiotic therapy. Trends Microbiol 21, 265–270. doi 10.1016/j.tim.2013.04.001

Thiele K., Wanner G, Kindzierski V, Jürgen G, Mayer U, Pachl F, Assaad FF (2009) The timely deposition of callose is essential for cytokinesis in Arabidopsis. The Plant Journal 58, 13–26. doi 10.1111/j.1365-313X.2008.03760.x

Tuteja N, Sopory SK (2008) Plant signaling in stress. Plant Signaling & Behavior 3, 79–86. doi 10.4161/psb.3.2.5303

van Doorn WG (2011) Classes of programmed cell death in plants, compared to those in animals. J Exp Bot 14, 4749–4761. doi 10.1093/jxb/err196

van Doorn WG, Beers EP, Dangl JL (2011) Morphological classification of plant cell deaths. Cell Death Differentiation 18, 1241–1246. doi 10.1038/cdd.2011.36

van Doorn WG, Woltering EJ (2005) Many ways to exit? Cell death categories in plants. Trends Plant Sci 10, 117–122. doi 10.1016/j.tplants.2005.01.006

Vescovi M, Riefle M, Gessuti M, Novák O, Schmülling T, Lo Schiavo F (2012) Programmed cell death induced by high levels of cytokinin in *Arabidopsis* cultured cells is mediated by the cytokinin receptor CRE1/AHK4. J Exp Bot 63, 2825–2832. doi 10.1093/jxb/ers008

Wang Y, Wu Y, Yu B, Yin Z, Xia Y (2017) EXTRA-LARGE G PROTEINs Interact with E3 Ligases PUB4 and PUB2 and Function in Cytokinin and Developmental Processes. Plant Physiol 173, 1235–1246. doi 10.1104/pp.16.00816

Watanabe N, Lam E (2011) Calcium-dependent activation and autolysis of Arabidopsis metacaspase 2d. J Biol Chem 286, 10027–10040. doi 10.1074/jbc.M110.194340

Wojciechowska N, Sobieszczuk-Nowicka E, Bagniewska-Zadworna A (2018) Plant organ senescence - regulation by manifold pathways. Plant Biol 20, 167–181. doi 10.1111/plb.12672

Zhang K, Letham DS, John PC (1996) Cytokinin controls the cell cycle at mitosis by stimulating the tyrosine dephosphorylation and activation of $p34^{cdc2}$-like H1 histone kinase. Planta 200, 2–12. doi 10.1007/BF00196642

Zhu P, Yu XH, Wang C et al (2020) Structural basis for Ca^{2+}-dependent activation of a plant metacaspase. Nat Commun 11, 2249. 10.1038/s41467-020-15830-8

Figure captions

Fig. 1. Response of tobacco BY-2 cells to 50 µM kinetin. **A** Time course of mortality for kinetin treatment from day 0 (Kin, d0), or from day 3 (Kin, d3) after subcultivation as compared to the untreated control (con). Data represent mean value from three independent experimental series scoring 600 individual cells per replication. **B** Representative cells stained with 4', 6-diamidine-2'-phenylindole dihydrochloride (DAPI) and viewed either at the peak of mitotic activity (day 3 after subcultivation), or at the time of maximal cell expansion (day 5 after subcultivation) either in control cells or cells treated with kinetin from day 0.

Fig. 2. Frequency distributions over DNA content per nucleus inferred from DAPI staining through the cultivation cycle in control cells (A), and in cells that had been treated with 50 µM kinetin from day 0 (B). The DNA contents (C) were classified into hypoploid cells (<2C), cells in G_1 phase (2C), cells in S-phase (2-4C), cells in G_2-phase (4C), and endopolyploid cells (>4C). Data represent mean and standard errors from two independent experiments consisting of three technical replications with a 600-800 individual nuclei per replication.

Fig. 3. Appearance of BY-2 after double staining with Acridin Orange (membrane permeable green signal) and Ethidium Bromide (membrane impermeable, red signal) in untreated controls, or addition of 50 µM kinetin at the time of subcultivation. **A** overview of the cells at day 3 or 7, respectively merging the signals from the green and red channels. B Cellular details of the stageing system used for classification in **Fig. 4**. *nco* nucleolus

Fig. 4. Frequency distributions over different stages of cell death as classified by double staining with Acridine Orange and Ethidium Bromide through the cultivation cycle in control cells (**A**), and in cells that had been treated with 50 µM kinetin from day 0 (**B**). The classification followed the system shown in **Fig. 3B**. Data represent mean and standard errors from two independent experiments consisting of three technical replications with a 350–400 individual cells per replication.

Fig. 5. Effect of kinetin on intracellular calcium levels reported by chloro-tetracycline. **A** Representative cells either at the peak of mitotic activity (day 3 after subcultivation), or at the end of the cultivation cycle (day 7 after subcultivation) either in control cells or cells treated with 50 µM kinetin from day 0. **B** Quantification of the fluorescent signal. Data represent mean and standard errors

from two independent experiments consisting of three technical replications with 50 to 100 individual nuclei per replication.

Fig. 6. Effect of kinetin on callose abundance at the cross-wall visualised by Aniline Blue. In either control cells or in cells treated with 50 µM kinetin from day 0. Data represent mean and standard errors from two independent experiments consisting of three technical replications with a 150–250 individual cells per replication.

Fig. 7. Graphical representation of Pearson correlation coefficients between cytosolic calcium (Ca^{2+}), accumulation of callose, the different stages of cell death and the nuclear DNA content in response to kinetin in tobacco BY-2 cells.

Fig. 8. Effect of kinetin on microtubules visualised by the marker TuB6-GFP and spinning-disc confocal microscopy either in control cells or in cells treated with 50 µM kinetin from day 0. Representative cells from the cell proliferation phase (day 2, **A-C**) or the cell expansion phase (day 5, **D-F**) are shown. Data represent geometrical projections collected separately for the cortical region (**A, D**) or the cell centre (**B, E**) in case of the control, or over the entire z-range in case of the kinetin treated cells (**C, F**).

Fig. 9. Effect of kinetin on actin filaments visualised by the marker FABD-GFP and spinning-disc confocal microscopy either in control cells, or in cells treated with 50 µM kinetin from day 0. Representative cells from the cell proliferation phase (day 2, **A, B**) or the cell expansion phase (day 5, **C, D**) are shown. Data represent geometrical projections.

Supplementary Data

Suppl. Fig. S1. Representative images showing the response of tobacco BY-2 cells to 50 µM kinetin (**A'-F'**) as compared to non-treated controls (**A-F**) at different days after subcultivation after staining with DAPI. Size bar 50 µm.

Suppl. Fig. S2. Fluorescence intensity histograms (**A-F**) and inferred frequency distributions of nuclear DNA content (**A'-F'**) in control cells (**A, A'**) and cells treated with 50 µM kinetin (**B-F**, **B'-F'**) sampled at different days after subcultivation.

Suppl. Fig. S3. Representative images showing the fluorescent calcium reporter chloro-tetracyclin reporting intracellular calcium levels in tobacco BY-2 cells treated with 50 µM kinetin (**A'-F'**) as compared to non-treated controls (**A-F**) at different days after subcultivation. Size bar 50 µm.

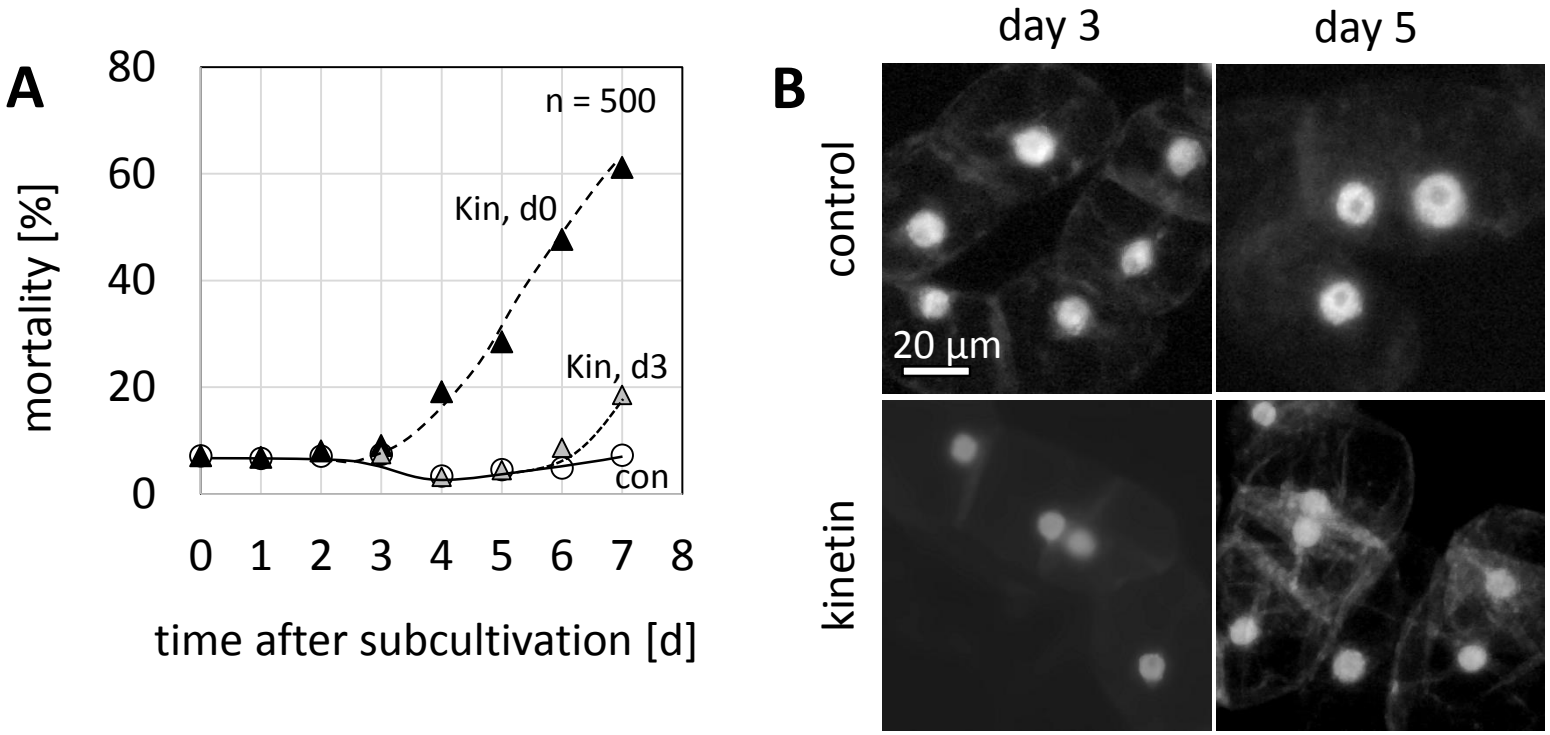

Figure_2

Click here to access/download;Figure;renamed_f5060.pptx

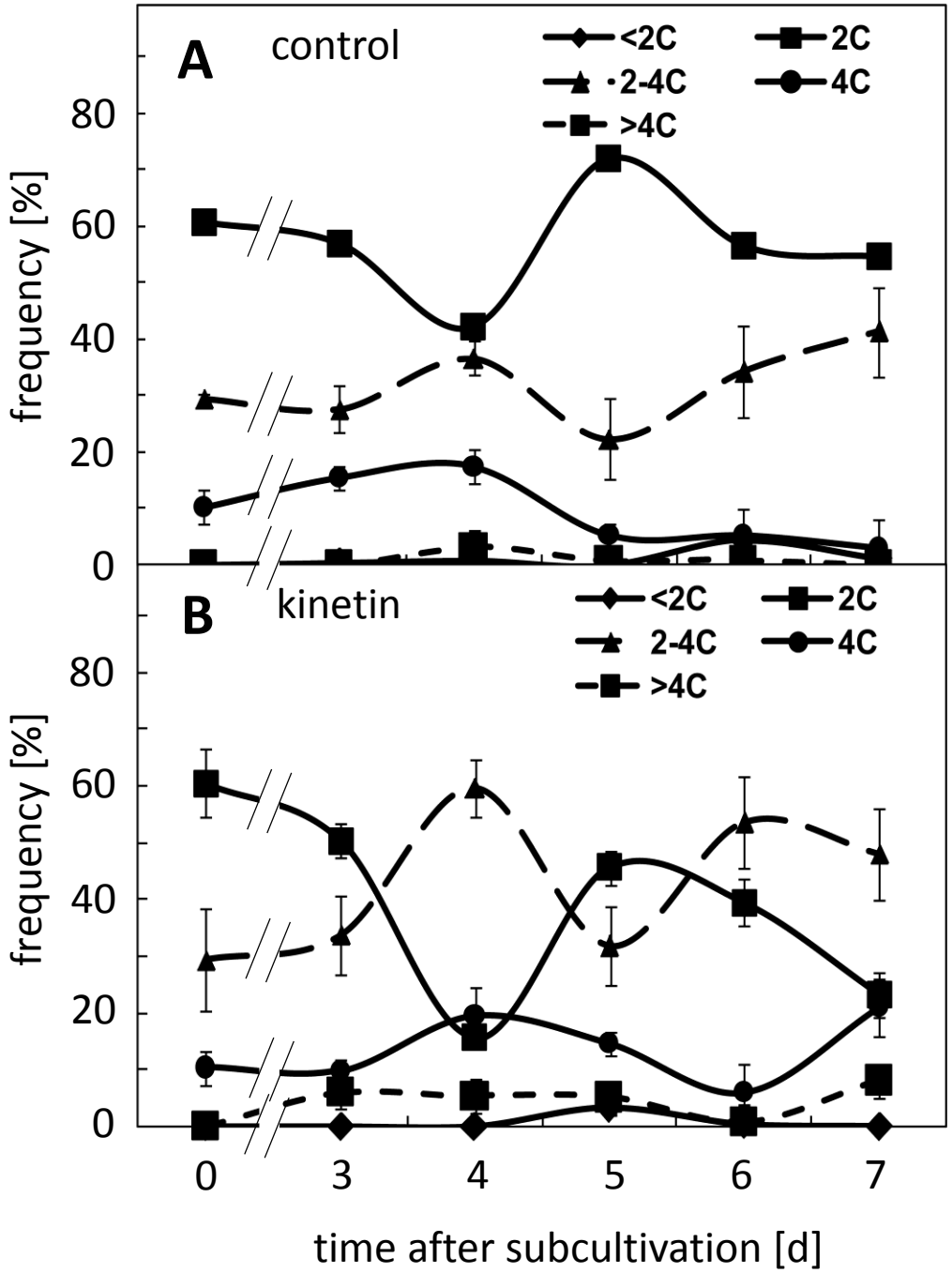

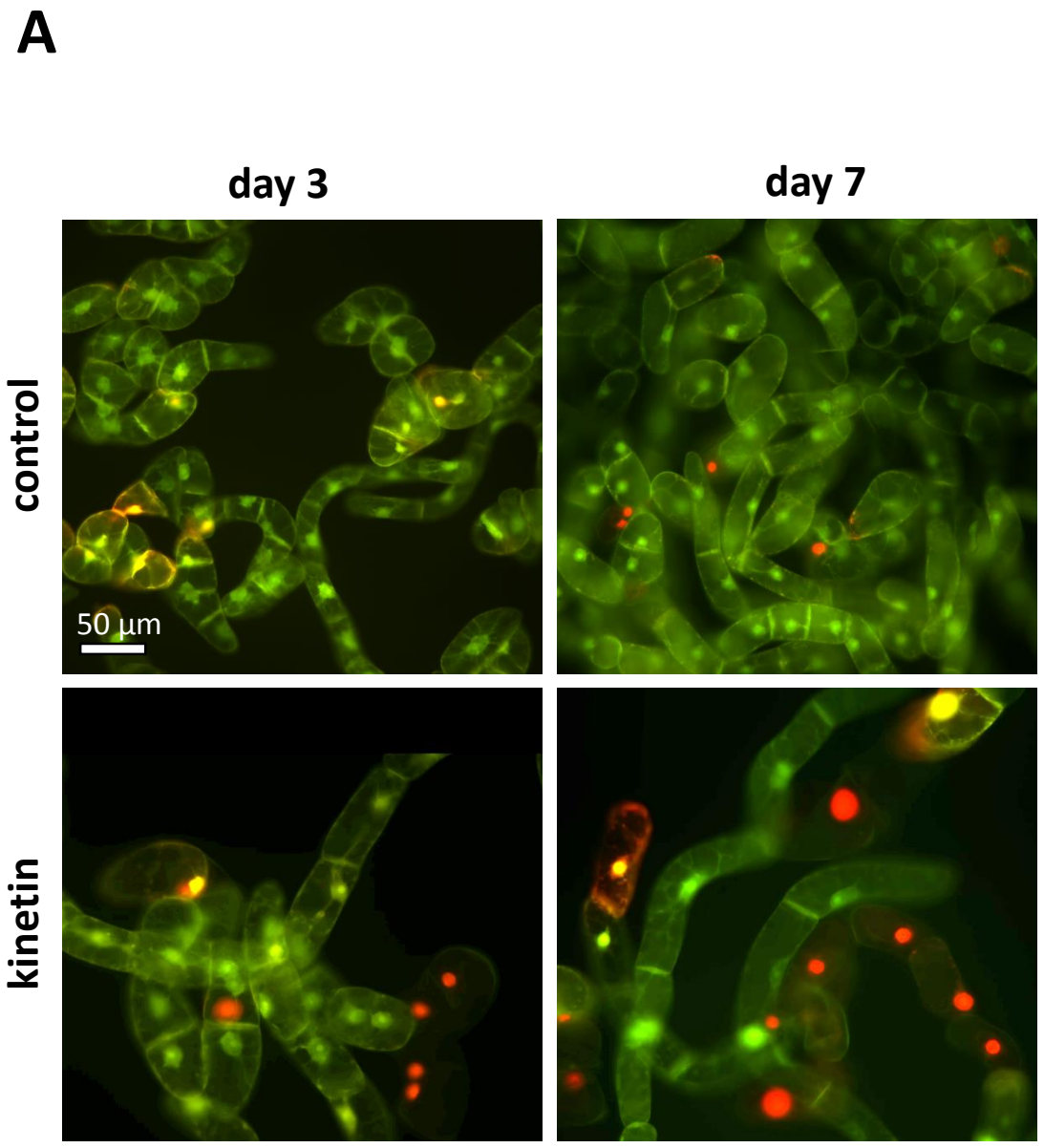

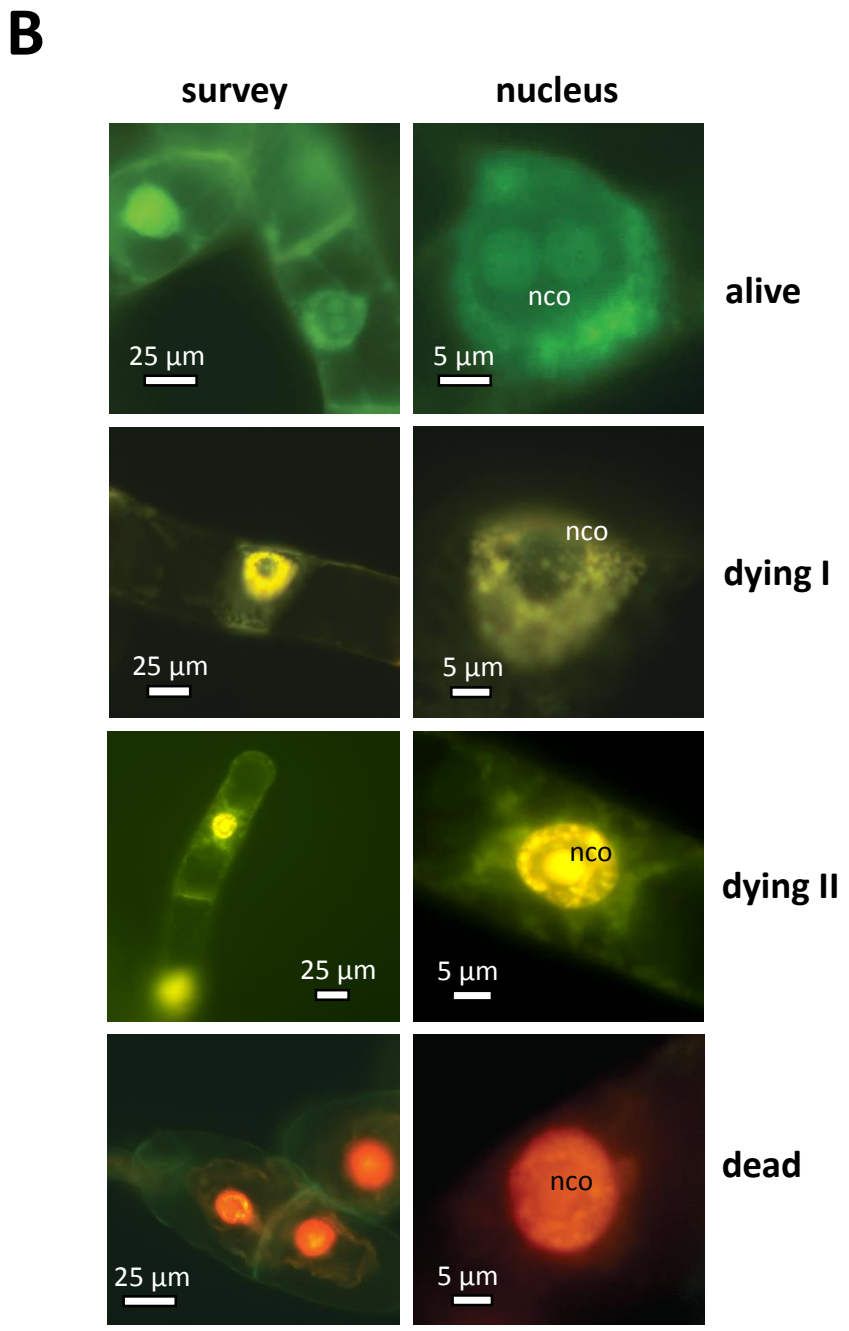

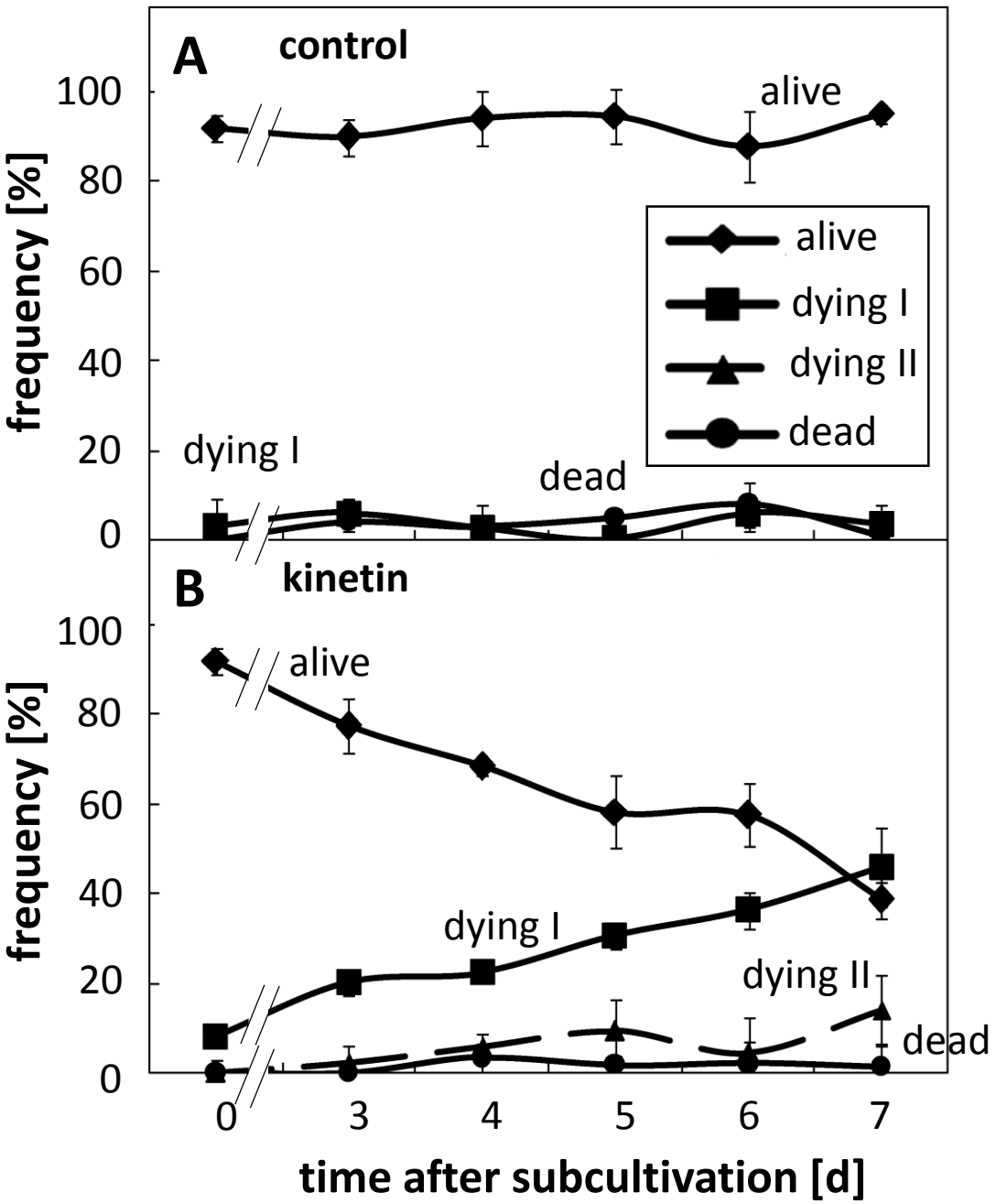

Figure_5

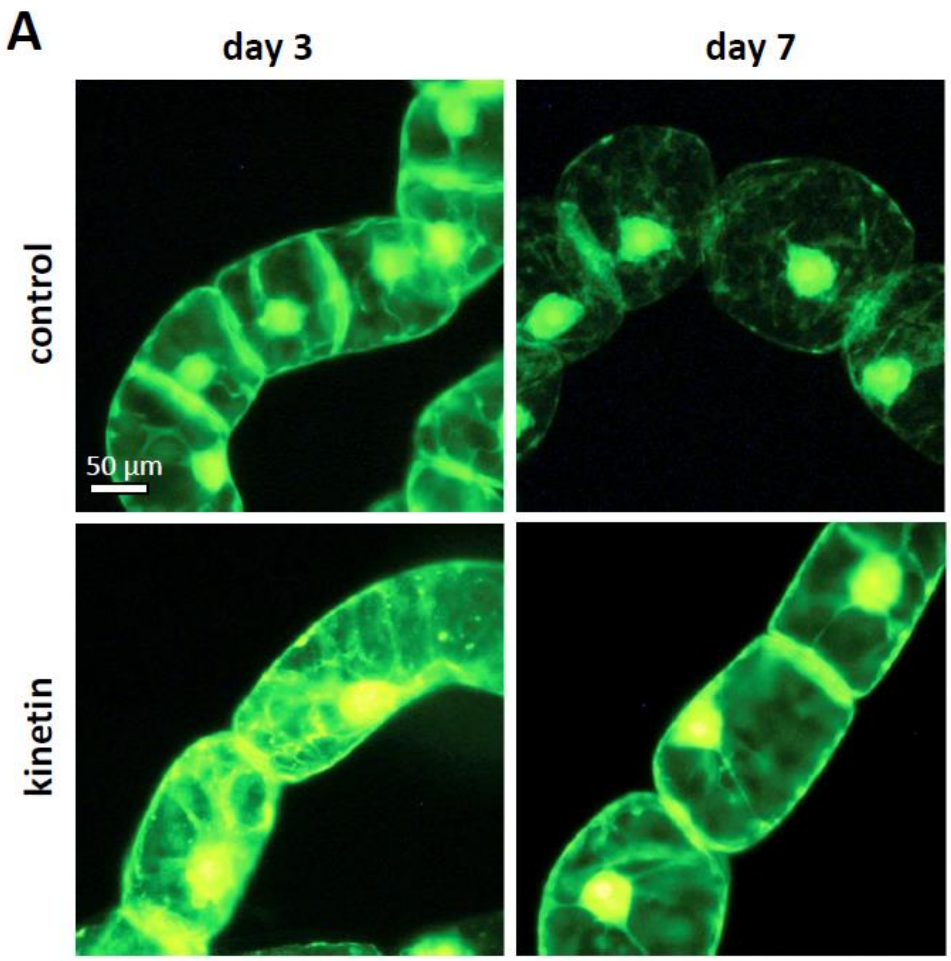

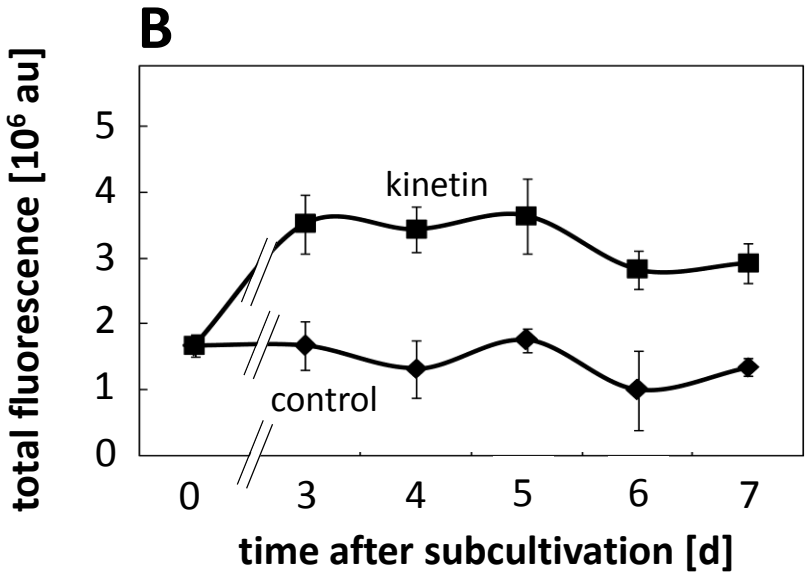

Figure_6

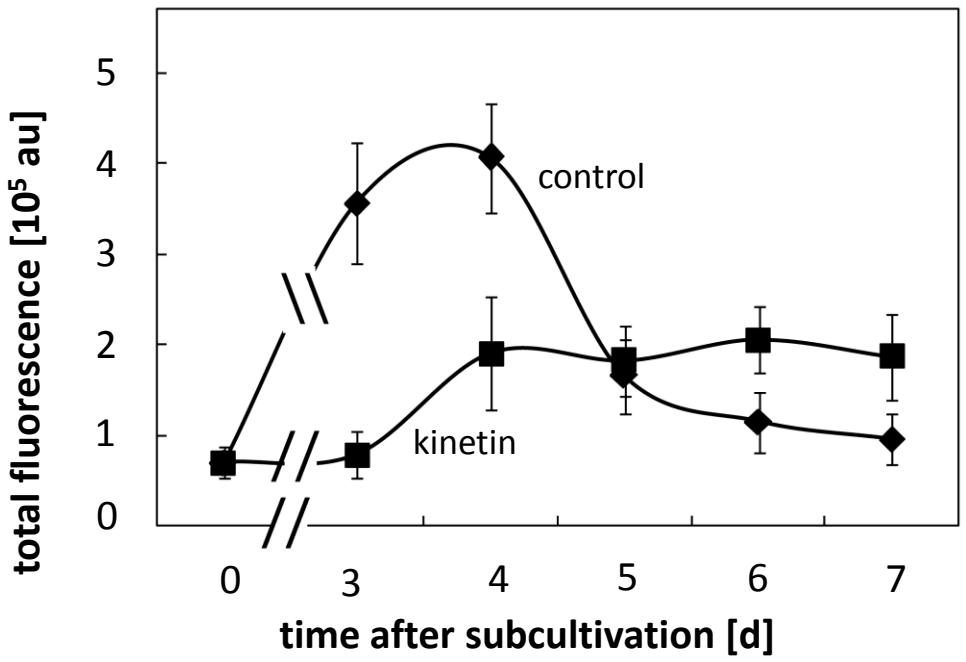

Figure_7

Click here to access/download;Figure;renamed_a2314.pptx

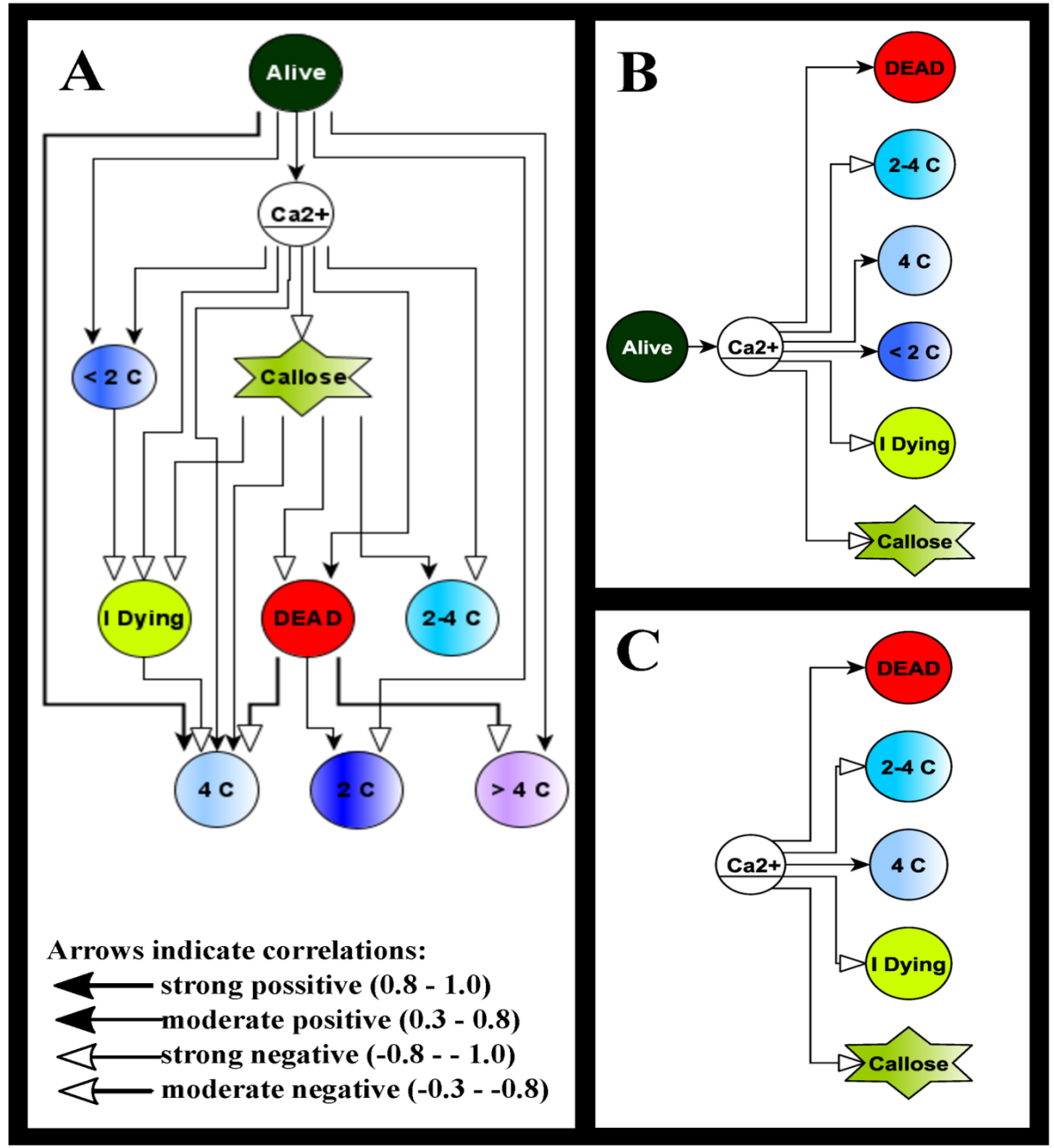

Figure_8

Click here to access/download;Figure;renamed_db12b.pptx

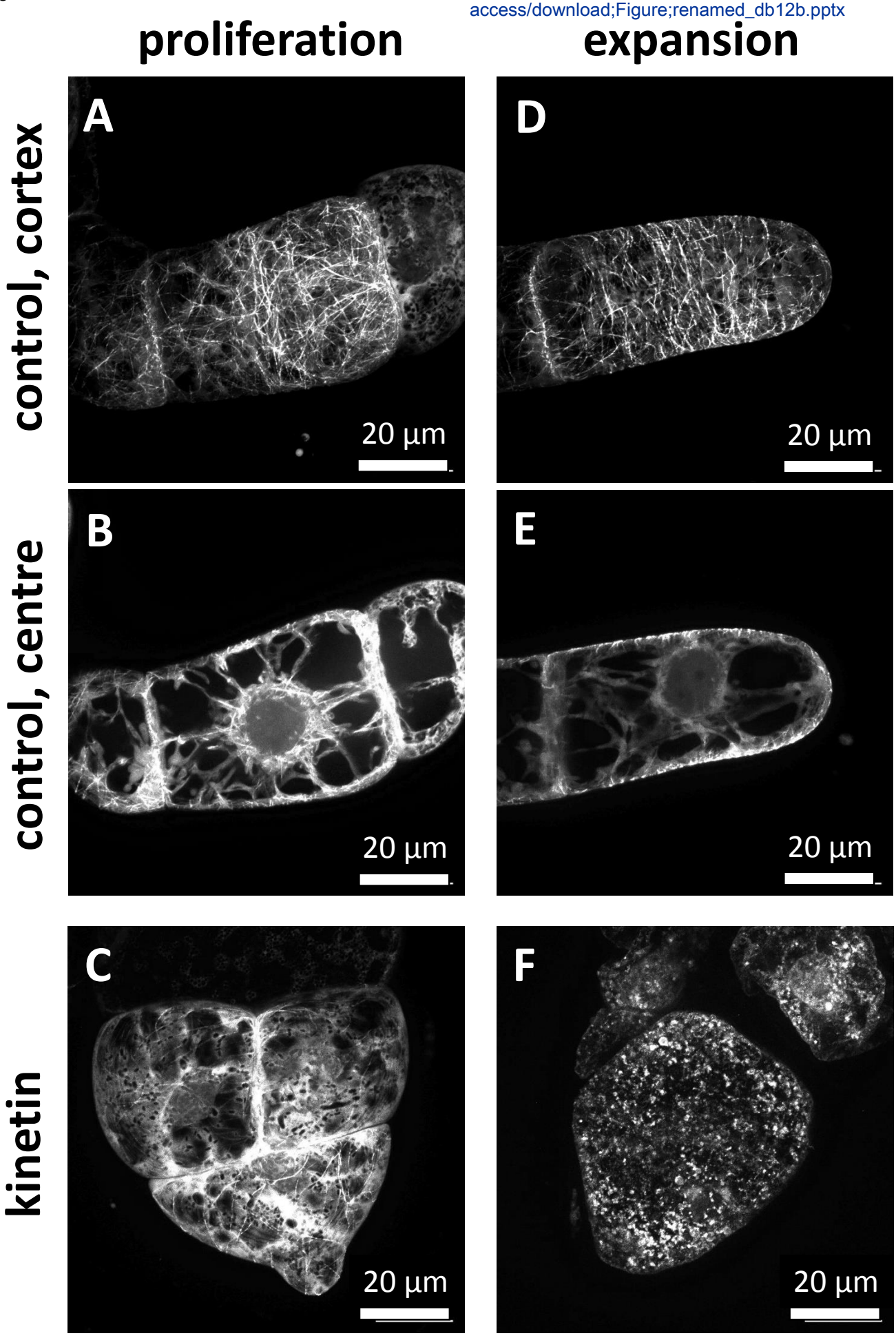

Figure_9

Click here to access/download;Figure;renamed_faf26.pptx

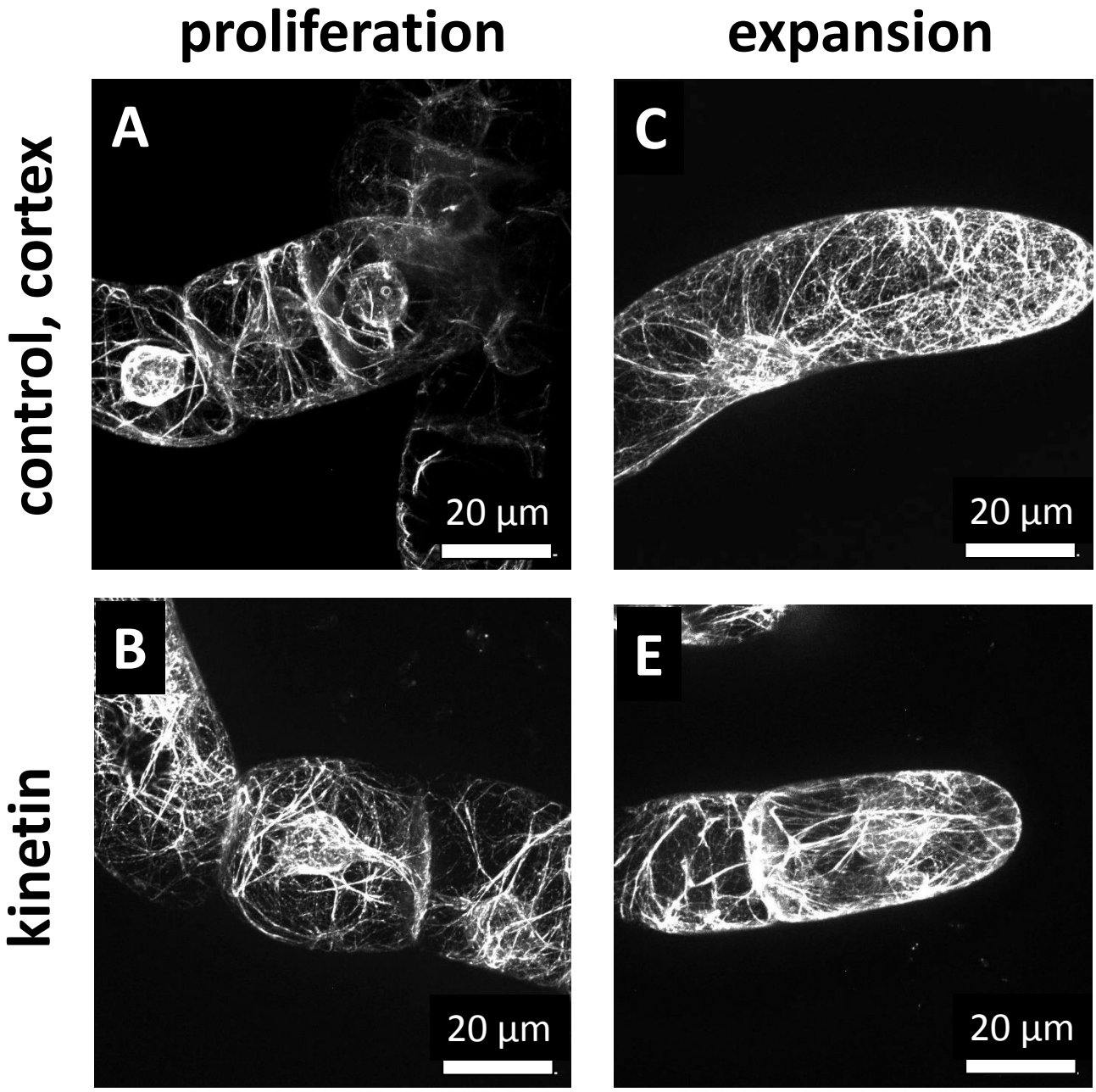

cover letter